CHAPTER

5

Challenges in crater chronology on Mars as reflected in Jezero crater

Lior Rubanenko[a,b,*], *Tyler M. Powell*[b], *Jean-Pierre Williams*[b], *Ingrid Daubar*[c], *Kenneth S. Edgett*[d] *and David A. Paige*[b]

[a]**Department of Geological Sciences, Stanford University, Stanford, CA, United States;** [b]**Department of Earth, Planetary, and Space Sciences, University of California, Los Angeles, CA, United States;** [c]**Brown University, Providence, RI, United States;** [d]**Malin Space Science Systems, Inc., San Diego, CA, United States**
***Corresponding author**

Abstract

The age of a planetary surface may be inferred from the size-frequency distribution of impact craters covering it. On Mars, the accuracy of this *crater chronology* technique may be compromised by past or present aeolian, fluvial, and pluvial erosion and sedimentation. Here, we review how these processes influence the crater age of the surface, employing as a case study the floor of Jezero crater, the landing site of the Mars 2020 Perseverance rover mission. We count craters and derive the retention ages of three prominent geologic units on the floor of Jezero, discussing some of the challenges faced during crater counting analysis. Our estimate for the retention age of the dark-toned floor unit is slightly younger compared to previous studies and is sensitive to statistical outliers. These factors should be taken into account when calibrating the crater age of the surface of the unit with its measured radiometric age.

1 Introduction

All solid planetary bodies in the solar system are scarred by craters of meteoritic origin, relics of the disc of debris that orbited the primordial Sun (Spencer, 1937). Cratered terrains record impacts integrated throughout their geologic lifetime. As a result, the size distribution of craters imprinted on a planetary surface may be used to constrain its age, assuming the impact rate over time is known (Baldwin, 1949; Kreiter, 1960). This method, termed crater chronology, is rooted in the assumption that the size-frequency distribution of craters on an initially smooth airless planetary surface closely follows the distribution of the impactors that formed them. However, many geologic processes impair our ability to perform crater chronology by affecting both the production of new craters and the removal of preexisting craters (Melosh, 1989; Neukum et al., 2001).

On the airless Moon, impacts are the main processes that affect craters' erosion and morphology

http://dx.doi.org/10.1016/B978-0-12-820245-6.00005-7

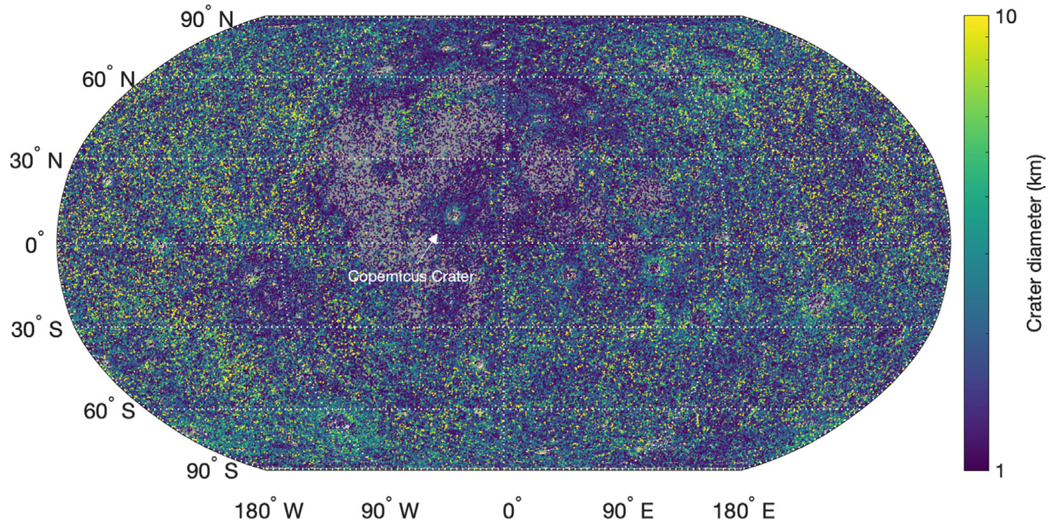

FIGURE 5.1 Impact craters >1 km on the Moon, color-coded by diameter on a logarithmic scale and stretched for emphasis (Robbins, 2019). Typically, the areal density of lunar craters varies as a function of the age of the surface. Locally, secondary craters may increase the number of craters on the surface, affecting its model-derived age (McEwen et al., 2005). For example, the dense population of secondary craters (secondaries; craters formed by fragments of the target material ejected by the primary impactor) around Copernicus crater (10°N, –20°E) makes the surrounding surface appear significantly older than other parts of the lunar Maria despite its younger age (Robbins, 2019). The range of crater diameter (stretched here for emphasis) demonstrates the typical crater size varies quite significantly for different regions, where craters in the younger Maria region tend to be slightly smaller (more purple) than craters in the highlands (more yellow).

through impact gardening by meteorites and overprinting by larger craters and ejected materials. In the past, volcanism also contributed to removing craters from the surface, mainly through burial. On Mars, the observed crater size distribution is also influenced by the planet's atmosphere. This includes not only atmospheric breakup and aeolian processes that can affect crater morphology over time (Ivanov et al., 1997; Popova et al., 2003) but also pluvial, fluvial, and sedimentary processes such as erosion by rivers, lacustrine sedimentation, or glacial activity that are only enabled by Mars' atmosphere [cite from the book: Viola+ 2020, Soare+ 2020, Gallagher+ 2020, Parker, 2020] and may bury or exhume impact craters (Milton, 1973; Lorenz and Lunine, 1996; Irwin and Zimbelman, 2012; Robbins and Hynek, 2012b). Consequently, while the size-frequency distribution of craters on the Moon typically varies as a function of the age of the surface (Fig. 5.1), on Mars, atmosphere-related processes may complicate this relationship. For example, note the latitudinal trend in both density and size distribution shown in Fig. 5.2, which may be caused by infill of small craters (Dobrea et al., 2020). These add to local variations in crater density due to the presence of secondaries visible, for example, near younger large craters such as Lomonosov crater (65°N, −10°E) or resurfacing by volcanism around Tharsis and Olympus Mons (eastwards of longitude 90°E, also see Fig. 5.3). The influence of secondaries on the primaries distribution may increase in environments where ground ice promotes relaxation and decreases primary crater retention.

The various processes that affect the observed crater size distribution on Mars gave birth to the concept of crater retention age (Hartmann, 1966, 2005) that represents the time during which craters of some diameter have accumulated and retained. This includes, in some cases, episodes of crater burial and exhumation (Malin et al., 2010).

In this manuscript, we review how the Martian environment affects the retention age of

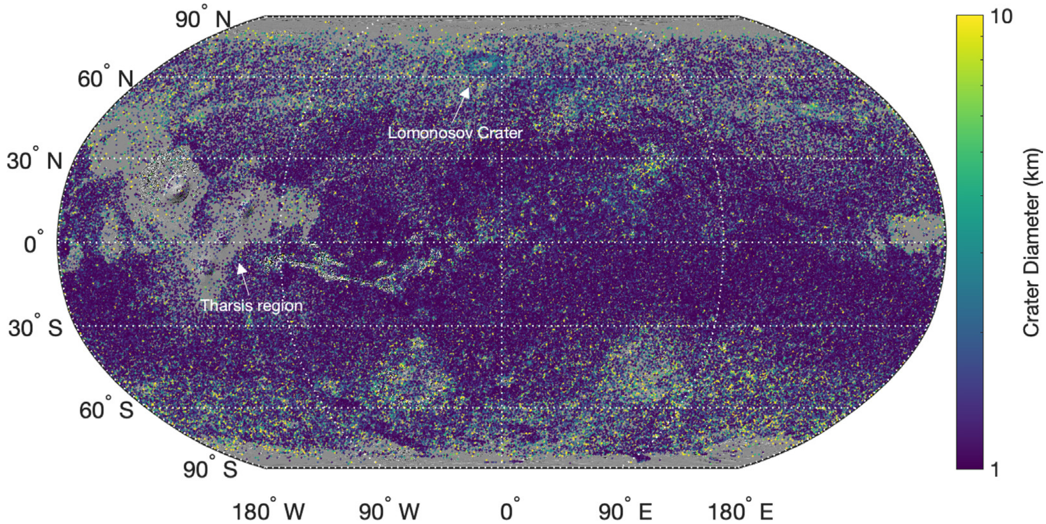

FIGURE 5.2 Impact craters >1 km on Mars, color-coded by diameter on a logarithmic scale and stretched for emphasis (Robbins and Hynek, 2012a). Compared to the airless and mostly geologically inactive Moon (Fig. 5.1), Mars shows evidence of volcanic (e.g., around Tharsis region) and atmospheric processes (e.g., ice near the poles) that change the crater areal density and size distribution both locally (such as around Lomonosov crater) and on larger scales.

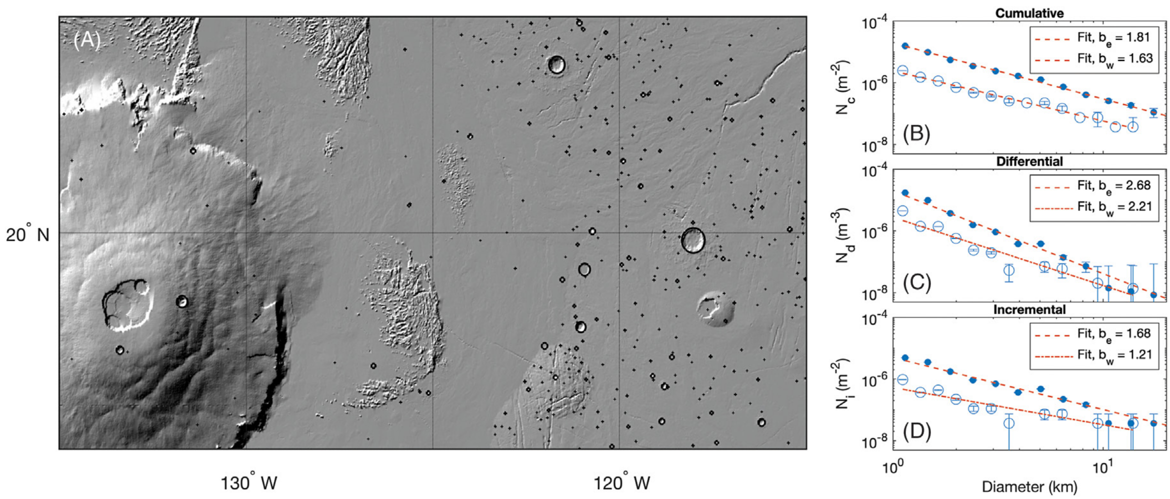

FIGURE 5.3 Shaded relief map (Smith et al., 2001) of cratered terrain that was recently resurfaced by volcanism, near Olympus Mons. (A) The lower crater density in the region closer to Mount Olympus (west of ~122°W, also emphasized by the dashed line) indicates a more recent or extensive resurfacing relative to the region further away from the mount. (B) Cumulative (C) differential, and (D) incremental size distributions with √2 logarithmic bin increments. Filled and empty circles show the distributions in the more heavily cratered region (east of the dashed line) and recently resurfaced region (west of the dashed line). b_e and b_w in the panels legends are the slope of the power law in log–log scale of the eastern and western crater distribution, respectively. Error bars are Poisson.

geologic units on Mars, focusing on Jezero crater, a ~40 km impact crater located in the Nili Fossae region of Mars, the landing site of the Mars 2020 Perseverance rover mission. Even before earning its name, Jezero crater was frequently cited as a textbook example for a developed Martian lacustrine system (Fassett and Head, 2005; Ehlmann et al., 2008; Schon et al., 2012; Goudge et al., 2012). The network of channels and valleys stretching hundreds of kilometers into the crater remain convincing evidence for extended periods of overland flow on Mars (Lapôtre and Ielpi, 2020). These rivers carried phyllosilicate clays, which are known to preserve organic matter, from the environment outside Jezero into a delta fan located near its northwestern rim. This makes Jezero a promising candidate to test the question of the past or present habitability of Mars. In addition, the rover is planned to collect core samples from the floor of the crater that will be retrieved and shipped to Earth by a future mission (Williford et al., 2018). Relating the absolute radiometric ages of different geologic units within Jezero to their crater-derived retention ages will serve to "calibrate" the planet's impact crater chronology. Consequently, constraining the crater age of the landing site and the surrounding region has implications for crater chronology determinations throughout the planet.

This chapter is intended to be accessible to readers inexperienced in crater chronology. We first review some basic concepts in crater chronology that will be employed throughout the text. Then, we present the geologic setting of Jezero crater and perform crater statistics on three prominent geologic units found within it. Finally, we discuss how the surface conditions on Mars may have affected the crater-derived age of these units.

2 Basic concepts in crater chronology

2.1 Theory

Nearly a century ago, astronomers proposed that the origin of craters on the lunar surface is meteoritic and not volcanic (Spencer, 1937). The formation process of craters from impactors may be broadly divided into three stages (Melosh, 1989). In the first *contact and compression* stage, the projectile transfers its kinetic energy to the target material and finally pushes and compresses it. In the second *excavation* stage, material is expelled from the point of impact by the nearly hemispherical shock wave. At the end of the excavation stage, a transient bowl-shaped cavity forms that is much larger than the impactor itself. This cavity is almost immediately altered by gravity in the last *modification* stage, and the crater obtains a final, shallower shape.

The comprehensive statistical analyses of cratered surfaces on the Moon compiled by Young (1940) and later by Kreiter (1960) and Hartmann (1964) provided the first quantitative evidence for the meteoritic origin hypothesis. These studies found the size distribution of craters ~10–100 km may be well described by a power law, similar to the size distribution of asteroids and terrestrial meteorites (Brown, 1960). Around the same time, Hawkins (1960), Anders (1965), Hartmann and Hartmann (1968), and others theorized collisional cascades between asteroids form power law–distributed impactor sizes, leading to power law–distributed impact crater sizes.

Adopting these ideas, c denotes the number of craters per unit area N with diameters $\geq D$ using a simple power law (Crater Analysis Techniques Working Group, 1979),

$$N(\geq D) = cD^{-b} \tag{5.1}$$

where b is the slope of the production function in log–log scale and c is a coefficient that translates the distribution vertically, along the y-axis.

These basic concepts are demonstrated in Fig. 5.3, where we show a cratered surface ear Olympus Mons in panel (A) and the corresponding crater cumulative size distribution in panel (B). The crater size distribution of the surface in panel (C) is well represented by a power law size distribution. As expected, the normalized cumulative count values of the more heavily cratered region are higher than those of the less heavily cratered region.

Another way to represent the number of craters on the surface is by using a differential distribution; the number of craters in some diameter bin, the width of which is dD, divided by the bin size,

$$\frac{dN}{dD} = bcD^{-(b+1)} = \tilde{c}D^{-(b+1)} \tag{5.2}$$

Yet another representation of cratered surfaces is called the incremental distribution, the absolute number of craters in a bin dD. The advantage of the incremental representation is that its slope, when using log-spaced diameter bins, is the same as that of the cumulative distribution. In panels (A) and (D) of Fig. 5.3, we show examples of a differential and an incremental distribution.

For a non-zero flux of impactors, the number of craters on an initially crater-free surface will increase with time. As a result, measuring the coefficient c of a crater power-law size distribution is—at least conceptually—similar to measuring the relative age of the surface. In order to obtain the absolute age, c must first be calibrated for surfaces whose age was derived employing methods such as radiometric or cosmic ray exposure age dating of samples collected on the Moon. By using models that describe the impactor size distribution across the solar system and their respective impact probabilities for each planet, these absolute measurements can be extended from the surface of the Moon to the surface of other planets (Ivanov, 2001; Stöffler and Ryder, 2001; Marchi et al., 2009; Le Feuvre and Wieczorek, 2011).

Initially, the production rate of craters will closely follow the impact rate. As time passes, newly formed craters will superimpose existing craters. At some point in time, the crater population will become so dense that *any* new crater formed on the surface will replace craters that occupy an area equal to the area affected by the new crater. This stage is termed crater saturation (sometimes termed equilibrium); even though new craters form on the surface, the observed crater density does not increase (Baldwin, 1981; Melosh, 1989; Neukum et al., 2001). We note that in many studies the term *crater equilibrium* describes a state in which craters are formed at the same rate they are destroyed by any surface process. To avoid confusion, we adopt the term saturation.

In many cases, crater saturation is described as a fraction of the *geometric saturation*, the number of craters that can be placed on an area fitted rim-to-rim in hexagonal close packing (Gault et al., 1974; Melosh, 1989). This stage may also be represented by a differential power-law coefficient ≈0.22.

With that concept in mind, it is useful to consider an additional mathematical depiction of cratered surfaces that would help identify saturation: the R-plot (relative plot). To obtain the R-plot of a crater population, we divide the incremental distribution by a power law with $b = 2$ (or the differential distribution by a power law with $b = 3$). In an R-plot, horizontal lines represent size distributions in which craters in every bin occupy the same fraction of the total area. As a result, the R-plot of surfaces in saturation will both be horizontal and have R values of 0.22. Increasing/decreasing R lines represent crater cumulative distributions, the incremental distribution exponent of which is $b < 2$ or $b > 2$, respectively. In panels (A)–(D) of Fig. 5.4, we show four example regions on Mars and the Moon. In panel (E), we show R-plots for these regions, which demonstrate their age difference and proximity to saturation.

2.2 Practice

The guiding principle of crater chronology is relatively straightforward; with time, older surfaces will experience more impacts and, as a result, will be more heavily cratered. This

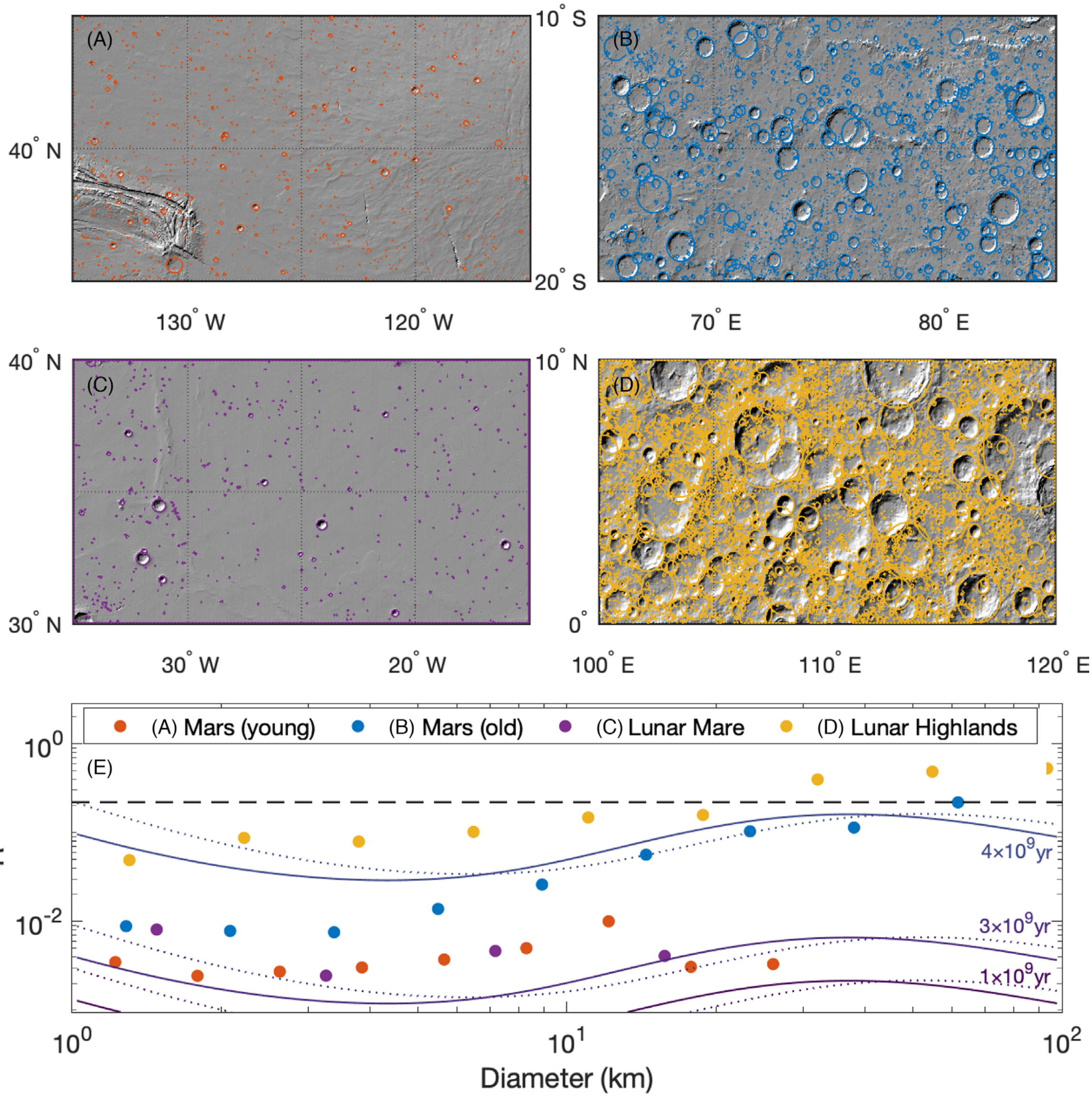

FIGURE 5.4 Four regions on the Moon and Mars showing different degradation states. (A) A region on Mars that was recently resurfaced showing lower crater density and smaller average crater diameter. (B) An older region on Mars shows the opposite. (C) A subset region of the lunar Maria. (D) A subset region of the lunar highlands, which is an example for a surface close to crater saturation (indicated by the *black dashed line*). (E) *R*-plots for the different regions, with isochrons derived from the Ivanov (2001) model for Mars (*solid lines*) and Neukum et al. (2001) model for the Moon (*dotted line*).

concept is well demonstrated in Fig. 5.3, which shows how the recently resurfaced region surrounding Olympus Mons is nearly devoid of craters >1 km compared to areas farther away from it, and Fig. 5.4, which compares cratered surfaces of different ages.

In order to determine the age of a surface, it is necessary to find the size distribution of the craters covering it. Traditionally, this *crater counting* technique is performed manually by first dividing the surface into homogeneous geologic units and recording the diameters of the visible craters within each unit (Greeley and Gault, 1970; Melosh, 1989; Neukum, 1984; Michael and Neukum, 2010). In recent years, this process is gradually being replaced by automatic detections that involve computer vision, machine, and deep learning techniques (Barata et al., 2004; Stepinski et al., 2009; Silburt et al., 2019). It is, however, important to note these algorithms often suffer from high false-positive and false-negative rates and consequently treated with suspicion by experienced crater counters.

Detailed studies of cratered surfaces have found that the power-law assumption stated previously does not always accurately capture the shape of the crater size distribution over large diameter ranges. This is in part due to the irregularities and the so-called knees in the size distribution of the asteroidal bodies that form them (Fujiwara and Tsukamoto, 1980; Rabinowitz, 1993; Stuart and Binzel, 2004). As a result, Neukum et al. (1975), Hartmann (1981), Neukum et al. (2001), Hartmann and Daubar (2017), and others employed crater counts to measure the size distribution of lunar craters and fit it with a piecewise power law or a series of polynomials that more accurately describe its features. These elaborate functions are termed *production functions* and have since been updated using more recent cratering data (Neukum and Ivanov, 1994; Hartmann, 1999; Marchi et al., 2009; Le Feuvre and Wieczorek, 2011; Williams et al., 2014) and observations (Brown et al., 2002; Mainzer et al., 2012). Over the years, these production functions have been adapted to date planetary surfaces for which we have no radiometric ages such as Mars, Mercury, and the moons of the outer planets (Ivanov, 2001; Bierhaus et al., 2005; Marchi et al., 2009; Le Feuvre and Wieczorek, 2011; Strom et al., 2011).

Graphically, production functions define lines termed isochrons, which represent the state of a crater size distribution at some point in time. For example, in Fig. 5.4E, we show how isochrons derived from the Ivanov (2001) production function can aid in dating planetary surfaces by matching them with a measured crater size distribution. Graphically, the size distribution represented by the red dots better fits the contour defined by the 10^9-year isochron, while the size distribution represented by the blue dots better fits the contour defined by the 3×10^9 year.

3 Challenges in crater chronology in Jezero crater

The methodology described earlier is idealized as it assumes only impacts can form and erode craters. However, many surface processes can disguise themselves as impact craters; it can be difficult to discern volcano pits, subsidence craters, and lava vents from craters formed by meteorites (Greeley and Gault, 1971; Blasius, 1976; Melosh, 1989). For example, the cavities in the bottom left corner of Fig. 5.3A not marked by black circles are the Olympus Mons summit caldera. At times, the geologic interpretation of what constitutes an impact crater may significantly affect the crater retention age estimates (Robbins and Hynek, 2012a). Additionally, spatial and temporal variations in bolide production or surface properties can change the production function and affect the morphology of fresh craters, and geologic and atmospheric processes may reduce the number of visible craters on various scales by burial, exhumation, infill, or erosion. Finally, on scales <100 m, fluctuations in atmospheric thickness may also affect the crater size distribution (Chappelow and Sharpton, 2006).

In the following section, we discuss how these complications are expressed in Jezero crater, the landing site of the Mars 2020 Perseverance rover mission.

3.1 The geology of Jezero crater

Nearly two decades ago, instruments onboard several Martian orbiters recorded a widespread network of valleys in the Nili Fossae region, leading into two deltaic deposits located near the northwestern wall of a ~40 km impact crater (18.4°N, 77.55°E) (Fassett and Head, 2005). Further, morphological analysis suggested the rivers that formed these valleys potentially filled the impact crater until its eastern rim was overtopped and breached, creating an outlet valley. These observations, along with earlier studies (De Hon, 1992; Cabrol and Grin, 1999), provided additional evidence for the existence of developed lacustrine systems on early Mars, earning the crater the name Jezero ("lake" in many Slavic languages).

In 2018 it was announced Jezero was selected as the landing site for the Mars 2020 mission (Grant et al., 2018). Jezero was selected mainly due to its distinct delta fan deposits that showed phyllosilicate mineral enrichment (Ehlmann et al., 2008; Goudge et al., 2017). The drainage basins for the deltas, which extends well into the Nili Fossae grabens, potentially funneled diverse minerals such as clays and organic materials into Jezero, making it a promising candidate to address the question of the past or present habitability of Mars (Goudge et al., 2015; Grant et al., 2018).

Detailed geomorphological analysis (Goudge et al., 2015) of Jezero and the drainage basin surrounding it revealed layered geology characteristic of lacustrine systems (Fig. 5.5). Within the crater the oldest layer is the rim and wall material which is covered in most places by dust. Small exposures reveal distinct spectra indicative of Mg/Fe-smectite. Stratigraphically above the rim and wall layer are the mottled terrain unit and the light-toned floor (LTF) unit, which is covered in many areas by dunes. The dunes covering the LTF unit present a strong spectral signature consistent with olivine, while the unit itself presents absorptions identified as hydrated carbonates, especially magnesite. Patches of the mottled terrain unit are found both inside the crater and in the surrounding region and are stamped with circular features likely to be degraded impact craters.

Perhaps the two most intriguing geologic units in Jezero crater are the north and west delta deposits (Goudge et al., 2015). These units, the sediment volume of which is estimated at ~5 km^3, were deposited in Jezero during the crater's stage as an extensive paleolake. The amount of material emplaced in the deltas implies the duration of inflow into Jezero lake was probably substantial (Fassett and Head, 2005; Lapôtre and Ielpi, 2020), testament of the climatic conditions in the Nili Fossae valley during the Noachian Period (Fassett and Head, 2005). Of the two deltas, the northern fan is more eroded than the western fan, which still preserves the inlet channel that once formed it.

The most pervasive unit on the crater floor is termed the volcanic floor unit (Goudge et al., 2015). This dark-toned, smooth layer was emplaced directly upon the LTF unit and was interpreted to embay the two delta fan deposits (Goudge et al., 2012). Spectroscopic analysis shows absorption near 1 and 2 μm, which may hint at the presence of olivine and pyroxene (Goudge et al., 2015). More recent studies have indicated the formation of the volcanic floor unit and its depositional history may be more confounding than previously thought (Golder et al., 2020; Kah et al., 2020; Baum and Wordsworth, 2020; Schuyler et al., 2020). To avoid the interpretive nomenclature, we call it hereafter the "dark-toned floor unit," taking into account these types of rock units can potentially be found to be sedimentary (Edgett and Malin, 2014).

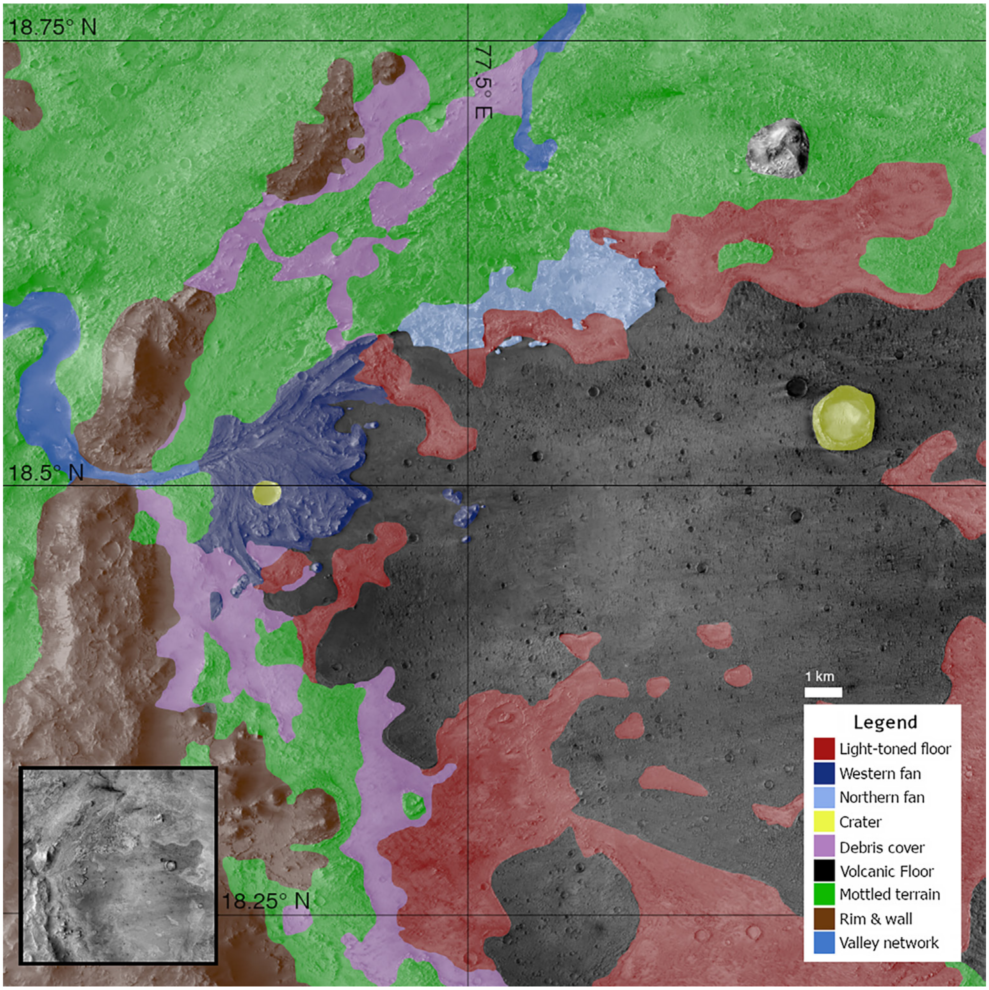

FIGURE 5.5 Jezero crater geologic map overlayed on a basemap of the Jezero crater mosaic captured by the Mars Reconnaissance Orbiter Context Camera (Malin et al., 2007). See Section 3.1 for a description of each geologic unit. Bottom left: grayscale minimap of Jezero crater. *Map was modified and enhanced from the original compiled by Goudge et al. (2015).*

Due to Jezero's stratigraphy, constraining the age of the dark-toned floor unit using crater statistics may help constrain the time in which its lake disappeared (Shahrzad et al., 2019). Somewhat fortunately, the unit appears to preserve continuous crater production, which may indicate its crater retention age will better correspond to its true (radiometric) age compared to typical Martian terrains.

3.2 Small crater statistics within Jezero crater

To perform our analysis, we compiled a catalog of craters within Jezero, nearly complete down to 50–70 m diameter, as measured by the deviation from power law. The purpose of this catalog is not only to provide information toward the future Mars 2020 mission, but also to demonstrate how various surface processes on Mars affect the age determined by crater chronology.

We first review four cratered geologic units within Jezero crater: the dark-toned floor unit, the western and northern delta units, and the light-toned unit. For each unit, we fit an age employing a crater chronology model appropriate for our diameter range. In the following section, we discuss the various geologic processes that may affect the age determined by the model, and how those may be addressed.

For consistency, we have elected to retain the names of the geologic units as they appear in previous works (Schon et al., 2012; Goudge et al., 2015, 2017), noting in some cases they may not reflect the true nature of the unit that are yet to be revealed by the Mars 2020 mission.

3.2.1 The dark-toned (volcanic) floor unit

Over the last decade, there has been some discussion over the age of the dark-toned floor unit of Jezero crater. Early works derived ages that differ by a factor of 2, from 1.4 Ga (Schon et al., 2012) to 3.45 Ga (Goudge et al., 2012). It should be noted these studies were not focused on Jezero but on Martian lacustrine systems in general and employed low-resolution imagery data that limited the size of counted craters. More recently, Shahrzad et al. (2019) were able to better constrain the crater age of the dark-toned deposit to 2.6 Ga using 187 craters with diameters >177 m.

Power-law statistics are sensitive to outliers. As a result, Shahrzad et al.'s (2019) age determination may be influenced by the small range of diameters they considered, which spans less than an order of magnitude. Additionally, given the thickness estimates of the dark-toned floor unit (10–30 m, Schon et al., 2012; Shahrzad et al., 2019), it is possible that some of the larger craters in their sample predate the emplacement of the dark-toned floor.

In order to reproduce the results of Shahrzad et al. (2019), we expand the analyzed diameter range by comparing image sets with different image saturation and illumination conditions obtained by the High Resolution Imaging Science Experiment (HiRISE, McEwen et al. (2007)). In total, we surveyed 2859 craters formed on the dark-toned unit, the diameters of which span two orders of magnitude: 5–670 m.

To perform our age analysis, we chose a contiguous area ~200 km^2, excluding "islands" belonging to other geologic units (see Fig. 5.5 for reference). We derive differential crater size distributions and fit them with a model (Hartmann and Daubar, 2017) employing Poisson timing analysis (Michael et al., 2016) using the *Craterstats* software package (Michael and Neukum, 2010). In Fig. 5.6, we show our crater map and derived differential crater size distribution, which is composed of two branches that follow different isochrons—possibly indicating recent resurfacing (see Section 3.3.1 for discussion).

In order to calculate the retention age of the dark-toned floor unit, we fit 925 craters 85–670 m with a chronology model appropriate for decameter-sized craters (Hartmann and Daubar, 2017). The range of crater diameters in our sample was chosen to include craters that would likely postdate the formation of the dark-toned floor unit based on its estimated thickness (10–30 m, Schon et al., 2012; Shahrzad et al., 2019) and the rollover diameter of the population. Assuming an initial depth/diameter ratio of 0.2, it is relatively safe to assume craters whose diameters <200–300 m do not predate the dark-toned unit.

To estimate the rollover diameter on the dark-toned unit, we employ bootstrapping as explained in Section 3.3.1. The age we determine for the dark-toned floor unit is 2.0 ± 0.07 Ga, slightly younger than the age obtained by Shahrzad et al. (2019) using the same model but a more restricted diameter range, 2.6 ± 0.2 Ga. It is important to note these ages most likely represent the crater retention age rather than the age of the unit (Hartmann, 1966). This is further discussed in Section 3.3.1.

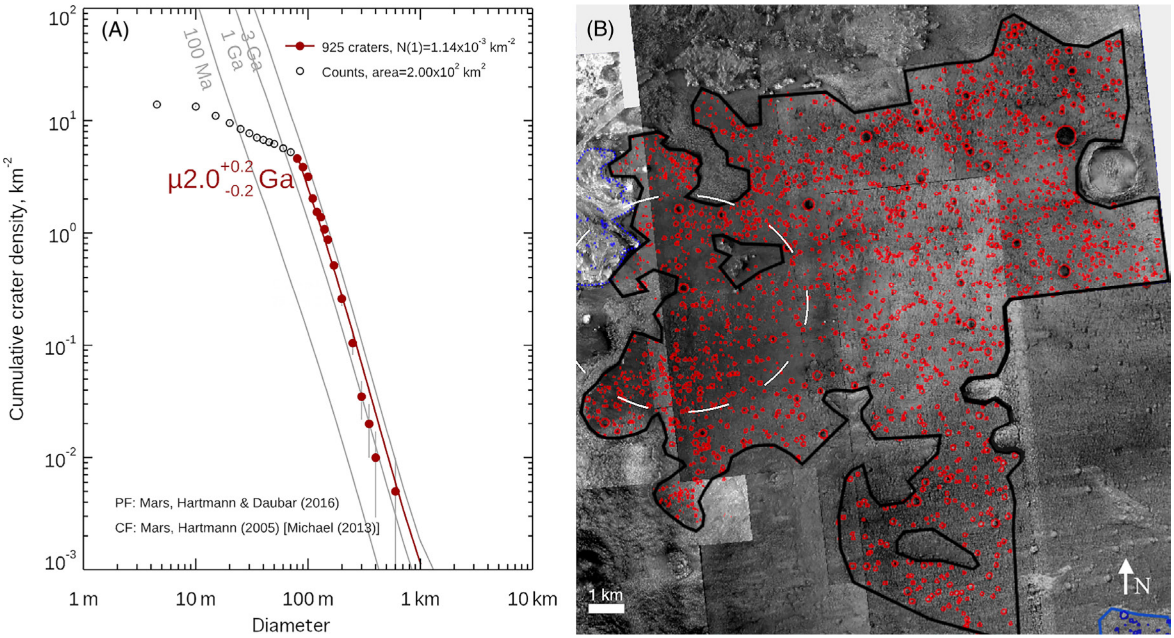

FIGURE 5.6 (A) Crater statistics on a subset region of the dark-toned (volcanic) floor unit of Jezero crater, close to the landing site ellipse near the western delta. By fitting a model age appropriate to our diameter range and Poisson timing analysis probability density function (Michael et al., 2016; Hartmann and Daubar, 2017), we derive an age estimate of ~2.0 ± 0.07 Ga. We only fit a model age to diameters greater than the rollover point (*filled circles*). (B) The spatial distribution of the craters on the dark-toned floor unit. The black line shows the edge of the subset region considered to make the differential plot in (A) and the white ellipse shows the approximate Mars 2020 landing site ellipse.

3.2.2 The northern and western delta fan units

Some of the stratigraphic evidence suggests both delta fan units precede the dark-toned floor unit, which embays them in many locations (Goudge et al., 2015). Unlike the dark-toned surface, the delta fans do not efficiently retain small craters, potentially due to the target material's higher susceptibility to erosion (Schuyler et al., 2020) or physical characteristics, which influence the crater dimensions during formation (see Section 3.3.4).

The double-branched size distribution of craters on the western delta fan of Jezero (~17 km^2) is likely evidence for aeolian resurfacing, which is indicated by many eroded and shallow (buried) craters on the unit. Belva crater, the largest crater on the delta unit, appears to postdate its formation and, most likely, indicates the unit is a few Ga old, in agreement with the eroded state of craters on scales 100–200 m and models of channel infill and subsequent erosion (Goudge et al., 2018; Salese et al., 2020). The smaller craters on the western delta unit approximately follow the 100-Ma isochron (Fig. 5.7) much like the craters on the dark-toned floor unit.

The northern delta fan is significantly more eroded than the western delta fan (Goudge et al., 2015). This unit shows little evidence for impact cratering, where the largest crater- like depressions are no larger than ~50 m. As a result, and while the geologic evidence suggests it is older than the dark-toned floor unit, the northern delta fan cannot be dated by using crater counting. For the same reason, the lower crater density on the northern delta does not

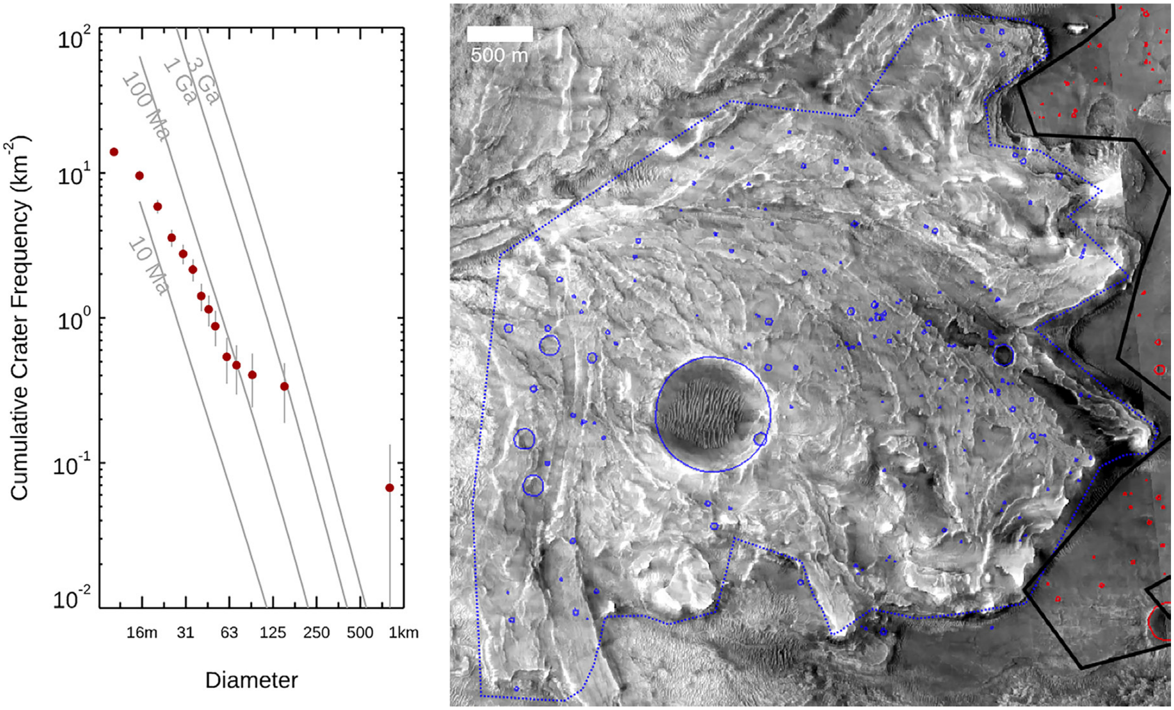

FIGURE 5.7 Crater statistics on the western delta fan unit, which does not preserve craters as well as the dark-toned (volcanic) floor unit.

necessarily imply it is younger than the western delta.

3.2.3 The light-toned floor

The extent of Jezero's delta fan units indicates the crater's lacustrine system has potentially been active for extended periods of time (Goudge et al., 2017). Consequently, it is not surprising that the spectroscopic analysis conducted by Goudge et al. (2015) and others found great diversity in the types of geologic units on the crater floor. Jezero's LTF is morphologically different than the dark-toned floor unit and is covered by several dune fields. To determine the retention age of this unit, it is necessary to find a subset region that contains craters that are large enough to survive erosion caused by the likely granular, dune-covered, target material, and subsequent aeolian erosion and burial. In Fig. 5.8, we derive the model age of the LTF using 232 craters on our chosen subset region, the area of which is 36.16 km^2. Other parts of the light-toned unit either were not as contiguous or did not have enough craters to perform a statistically significant age estimate. We find that while the depositional age of the unit is greater than that of the dark-toned floor unit, its model age is slightly younger, 1.7 Ga. This demonstrates well the concept of retention age (Hartmann, 1966) where the crater age of the surface is affected by processes that occurred (or are still occurring) after the surface had formed.

The differential crater size distribution on the LTF unit reveals again craters that follow two different isochrons. It is interesting to note that the younger branch of the distribution (at smaller diameters) follows a similar isochron to the one followed by the branches of the dark-toned floor

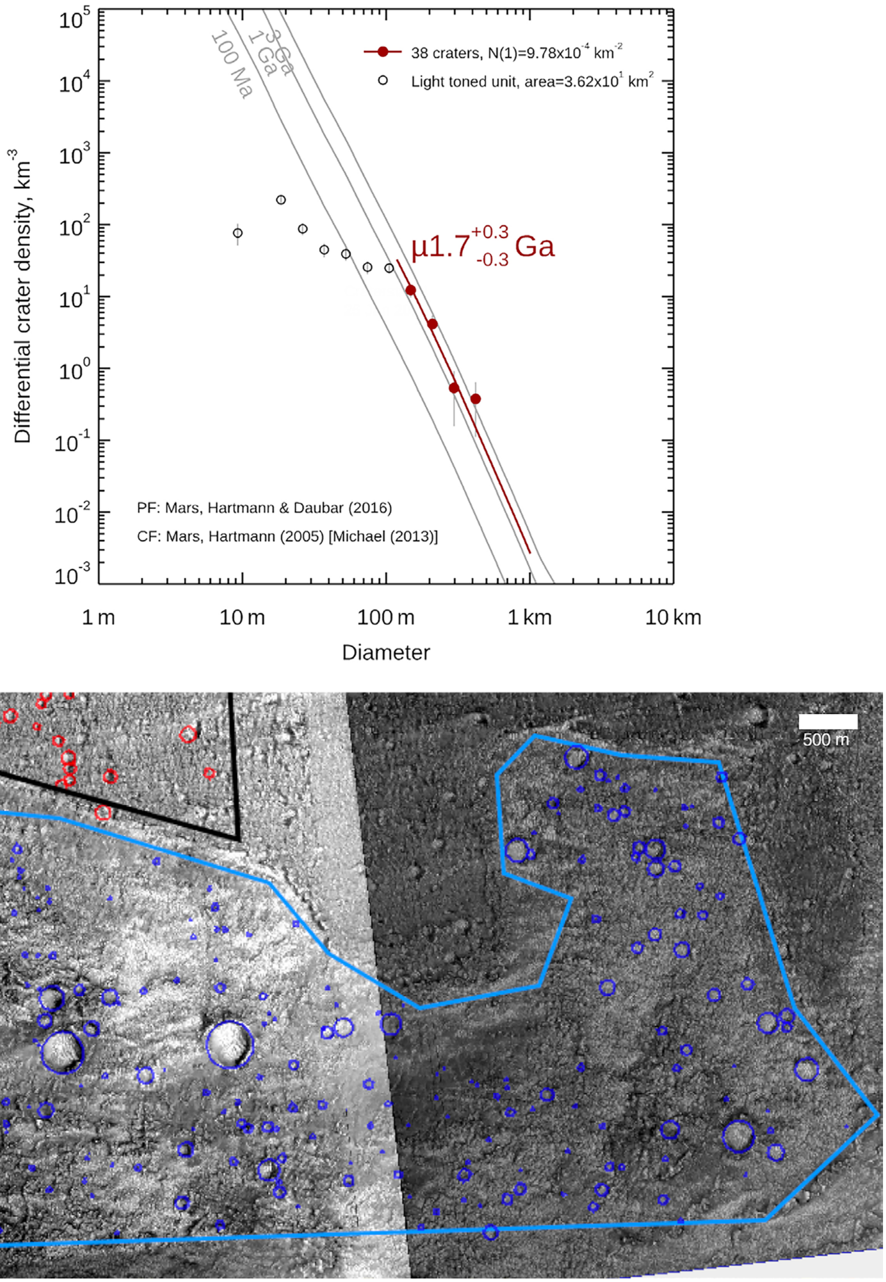

FIGURE 5.8 Crater statistics on the light-toned unit. Much like the delta fan units, the light-toned unit does not preserve craters well due to its extensive dune field.

unit and the delta floor unit. The potential implications of this observation will be discussed in the next section.

3.3 Analysis: challenges in crater chronology within Jezero crater

3.3.1 How do conceptual challenges in crater chronology affect the modeled age?

The age difference (~0.5 Ga) between our analysis and the one performed by Shahrzad et al. (2019) using the same chronology and production functions does not necessarily suggest disagreement. Rather, it emphasizes a fundamental challenge in crater chronology—that only rarely will two crater counting efforts return the exact same result. This is especially true within more limited regions that are sensitive to erosion, such as Jezero crater.

The floor of Jezero crater is a textbook example of some of the challenges in crater counting on Mars, where aeolian landforms often create closed shapes (in map view) that imitate the circular shape of craters. In Fig. 5.9, we annotate a few of these features, which resemble impact craters in their general shape. Even though these features could be identified as craters, careful examination shows their walls are a part of the elongated aeolian features that cross the scene diagonally from top to bottom. This example emphasizes crater counting is often prone to observation biases and personal experience (Greeley and Gault, 1970). As a result, it is important that a rigid set of criteria is defined during

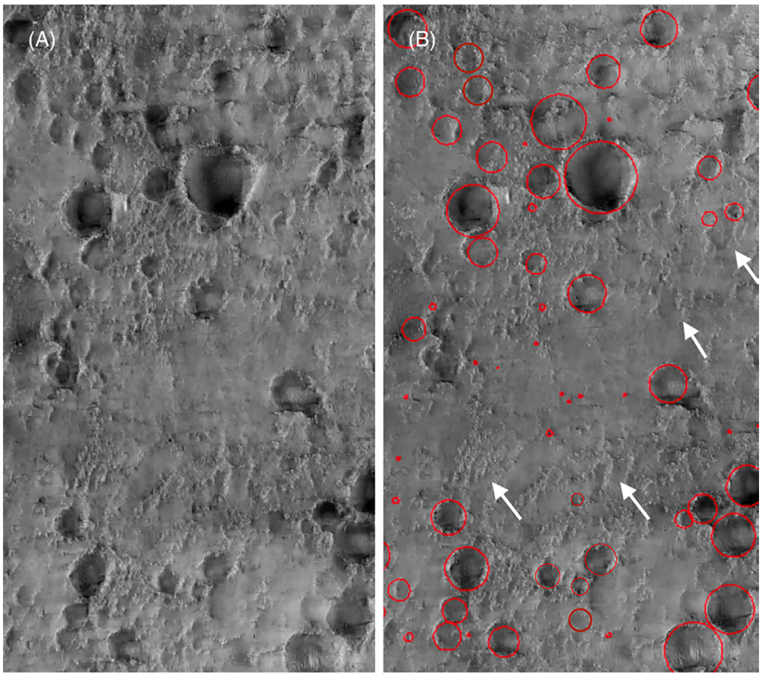

FIGURE 5.9 Distinguishing between impact craters and other depressions with a closed shape in map few is often difficult and may pose a serious challenge in the data collection (crater counting) stage. *Red circles* show features identified as impact crater by comparing several HiRISE images. *White arrows* show a few examples of features that may resemble craters but were not counted in our survey. Our criteria for identifying depressions as impact craters are a closed, circular shape in map view and smooth floor. For example, the flat depression at the center left border of the image may be a heavily eroded, infilled crater—but was not counted as one.

crater chronology studies, which defines what feature to classify as impact craters. For example, our criterion for classifying a depression as an impact crater is a closed shape (in map view), circular (or nearly circular) rims, and a smooth floor. To further rule out false positives, we compared several HiRISE images taken in different illumination conditions.

Different classification criteria may lead to different age determination, even when using the same model. To demonstrate this, we fit craters in the diameter range considered by Shahrzad et al. (2019) with the same chronology model as earlier, this time removing seven craters that only loosely match our classification criteria. In Fig. 5.10, we show these craters along with the fitted cumulative plot model age, which shows removing them from our sample decreases the modeled age by 200 Ma. When removing the same features from our original fit that contains a greater number of small craters, the fitted age only changes by ~1%.

Having said that, and since this study focuses on challenges in crater chronology, it is worthwhile to discuss how the Shahrzad et al. (2019) methodology differs from the one we employed here. In their survey, Shahrzad et al. (2019) noted the lower limit for considering craters useful

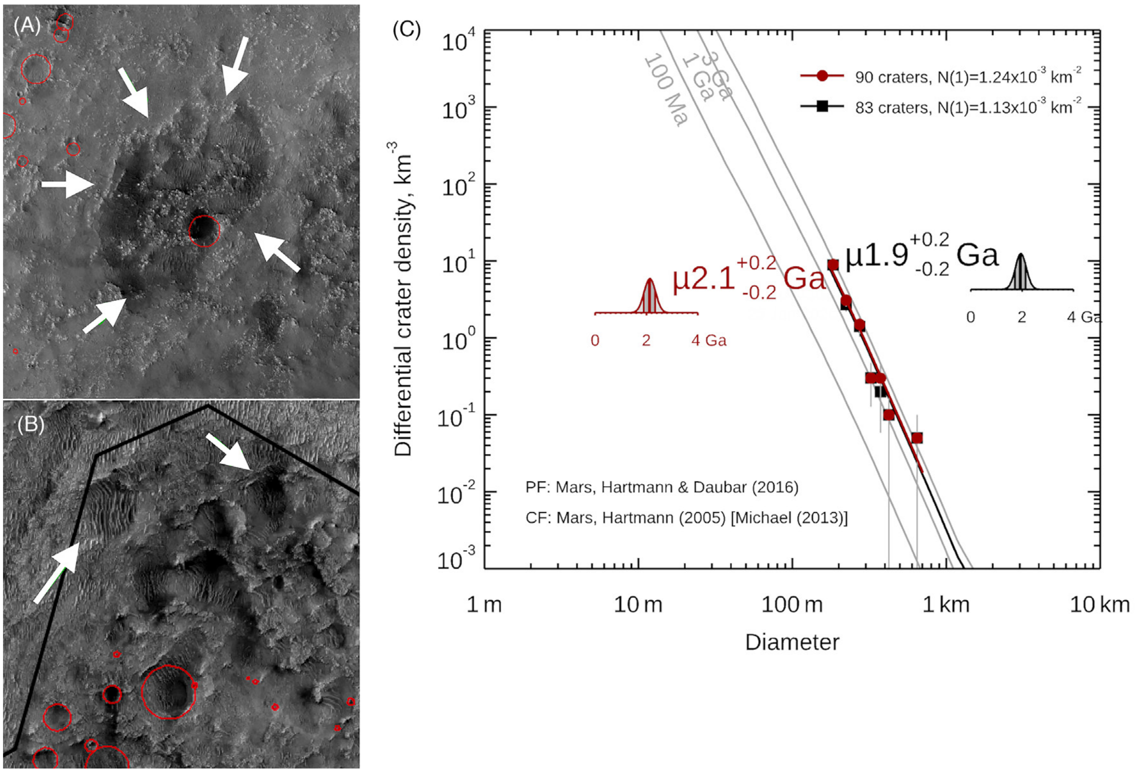

FIGURE 5.10 Including small craters in age determination can help resolve classification ambiguities that affect the model age. (A) and (B) Depressions ruled out as craters (*white arrows*) in this study but counted as craters in previous studies (Shahrzad et al., 2019). (C) Here we show that if the sample only includes craters >177 m [as in Shahrzad et al. (2019), however, counted over a smaller region], removing seven ambiguous depressions [panels (A) and (B)] that may be classified as craters change the model age (*red vs. black lines*) by 10%. If the same seven large craters are removed from the fit in Fig. 5.6 that contained an order of magnitude more craters, the modeled age does not change.

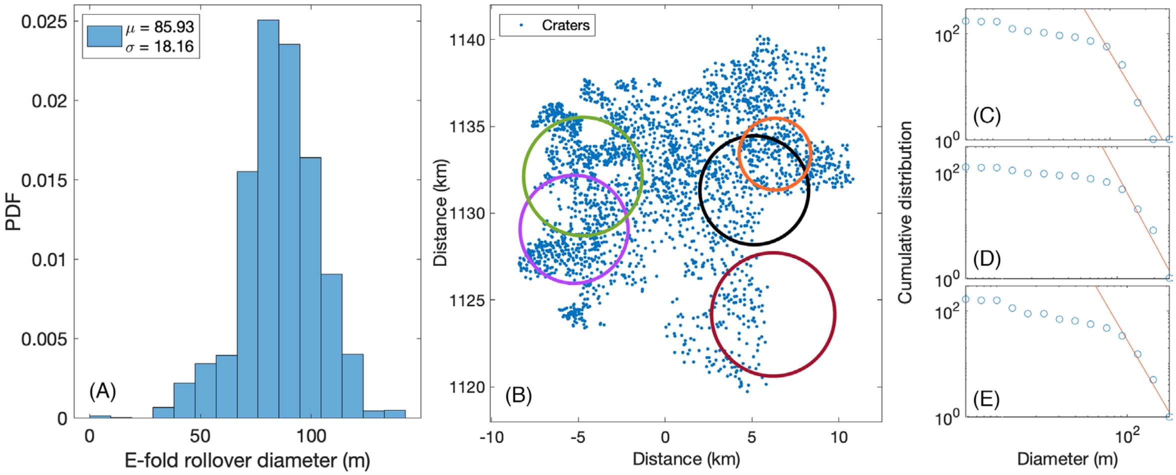

FIGURE 5.11 We constrain the rollover diameter of the crater size distribution using bootstrap analysis to be ~85 ± 18 m. (A) The distribution of the rollover diameters over 5000 iterations, each containing at least 50 craters. Values in legend indicate the mean and standard deviation of the bootstrap distribution. (B) The spatial distribution of craters within Jezero's dark-toned (volcanic) floor unit. Circles show a few example iterations of our bootstrap model used to cookie-cut craters and make the distribution in panel (A). (C)–(E) The power-law size distribution for several example iterations. We first fit a power law to the right-hand branch of the size distribution and calculate the difference between the fit and size distribution. The rollover diameter is estimated as the diameter in which this difference decreases e-fold.

for dating is not a factor of the image resolution (a few m/px) but of small-scale geological processes that accelerate crater erosion. Based on the rollover diameter of three subregions of the dark-toned floor unit, they found the crater size distribution deviates from the production function between 50 and 100 m and concluded that counts of craters <100 m are significantly affected by erosion or coverage. As a result, and due to additional spatial non-uniformity more prevalent in smaller craters, they only counted craters >177 m. This limited diameter range may affect the derived crater age of the dark-toned floor unit not only because it increases the variance associated with a smaller sample size, but also since some of the counted craters, the depth of which is equivalent to the estimated thickness of the unit (10–30 m, Schon et al., 2012; Shahrzad et al., 2019), could have, in theory, preceded the unit's emplacement.

In an attempt to increase the survey diameter range and achieve more statistically robust results, we constrain the rollover diameter of craters using bootstrapping (Efron and Tibshirani, 1985, see also Fig. 5.11). Bootstrapping is a well-known statistical method for measuring the properties of estimators of a dataset by randomly sampling it with replacement. Instead of describing the data using a single value, bootstrapping could add information about the spatial variability of the sample bias or variance.

We create circular Boolean masks, the radii and position of which are drawn from a uniform distribution. We first choose the circle radius between 3 and 5 km, and then randomize its position such that its entire area is contained within the floor unit. In each of the 5000 bootstrapping iterations, we calculate the rollover diameter defined as the e-fold difference between the power-law part of the size distribution and the part deviating from that power law. We discard bins with <50 craters. In Fig. 5.11, we show the mean rollover diameter based on our analysis is ~85 ± 18 m and consequently choose to use craters >85 m. Our method could be utilized as a robust estimate of the rollover crater diameter in other cases.

3.3.2 *Is the dark-toned (volcanic) floor unit contaminated by secondary craters?*

The areal density of craters on the dark-toned floor unit varies quite significantly, with what appears to be a decreasing east-west density gradient (Fig. 5.12A). The higher crater density in the northeastern part of the dark-toned floor was also noted by Shahrzad et al. (2019), who suggested a few possible causes, among which is contamination by secondary craters.

The question of whether contamination by secondary craters can potentially affect the surface age derived from crater chronology is an actively researched topic in planetary sciences. Observations conducted by Shoemaker (1965) on Mare Cognitum on the Moon have revealed a production function, the slope exponent of which for craters <1 km is significantly steeper than the average slope in the lunar mare previously estimated by Hartmann (1964) and others for craters >1 km. Later studies (Wilhelms, 1976; Schultz and Singer, 1980) further explored the spatial characteristics of secondary craters clusters and found a significantly steeper slope of ~4 and a shallower, more elliptical morphology due to the typically more oblique impact angle and generally lower impact velocity. Due to the steeper slope of the secondary size distribution compared to the primary size distribution, it was speculated that secondary craters could be significantly more numerous at smaller sizes than primary craters and affect the modeled age (Shoemaker, 1965; Soderblom et al., 1974).

During the past two decades, studies have suggested some km-sized craters on Mars such as Zunil crater (~10 km) may produce up to tens of millions of secondaries that extend hundreds of crater radii away from the primary impact (McEwen et al., 2005; Preblich et al., 2007). While this somewhat alarming result seems to imply secondaries may have a large cumulative effect on the average crater size distribution, more recent analyses have concluded that the majority of secondary craters on the Moon and Mars form close to the primary crater or along rays (Quantin et al., 2016; Williams et al., 2018; Bierhaus et al., 2018). However, the contribution

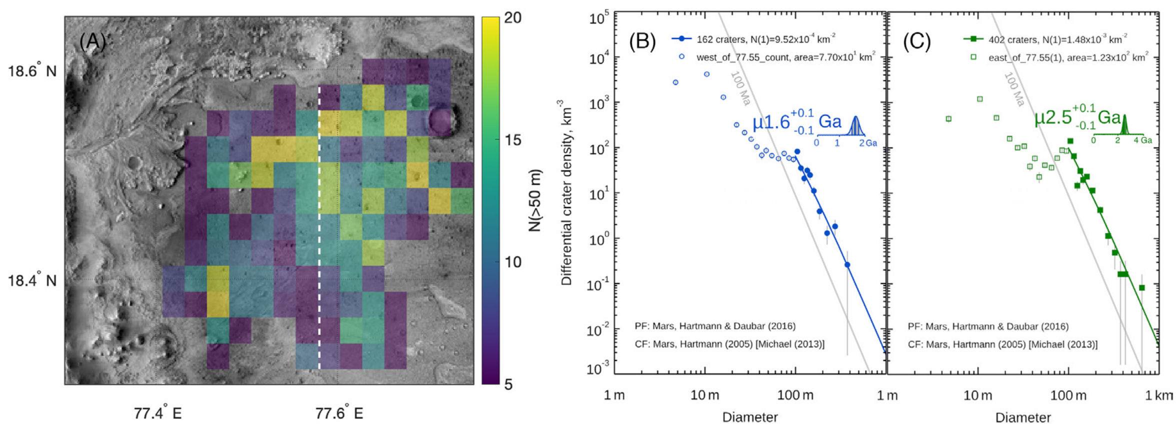

FIGURE 5.12 Variations in crater size distribution across the dark-toned (volcanic) floor unit. (A) The density of impact craters >50 m on the mafic floor unit is higher in the northeastern part of the basin divided into equal-area bins ~1 × 1 km. (B) and (C) Differential distribution of craters in the western side (B) and the eastern side (C) of the dark-toned floor unit, also emphasized by the white dashed line. The eastern and western crater size distributions are different both in the absolute crater density, but also in the average crater diameter, which is nearly double in the eastern side. Using the Kolmogorov–Smirnov test, we reject the null hypothesis that the craters from both sides of Jezero originate in the same distribution ($P < 0.01$).

of distant secondaries to the crater production function is still unclear. This topic is reviewed in depth in (Chapter 6: The Role of Secondary Craters on Martian Crater Chronology).

We verify the observation that craters on the eastern side of the dark-toned floor are denser than craters in the western part using a Kolmogorov–Smirnov (K-S) one-tailed test (Massey, 1951), and reject the null hypothesis that craters in two sides of the floor unit come from the same distribution [$P < .01$, also compare lines in panels (B) and (C) of Fig. 5.12].

It appears both visually and statistically that the crater density is higher in the eastern part of the dark-toned floor unit, but the reason behind this higher density is puzzling and poorly understood.

The craters in the northeastern part of the dark-toned floor unit do not resemble a field of secondary craters, with no immediately identifiable clusters or crater chains. Additionally, craters in that area do not appear to be more elliptical or shallower compared to other parts of the unit [see examples for distinctive secondaries fields in Robbins and Hynek (2011)] and it does not appear that Jezero crater is located near a large recent primary crater that may have contaminated it with secondaries (Robbins and Hynek, 2014). However, contamination by secondaries ejected from more distant basins cannot be completely ruled out.

Visually, the region with lower crater density in the western part of the dark-toned floor unit resembles the eroded delta fragments in tone and smoothness more than it resembles the dark-toned floor unit in the eastern, more heavily cratered side (Fig. 5.13). This leads us to speculate the reason for these patches of low crater density is that they were exhumed from underneath the delta deposits which eroded and disappeared with time, or that increased aeolian erosion on the western side of the crater removed material from the delta fragments (blue islands near the center of Fig. 5.5) onto the volcanic floor unit,

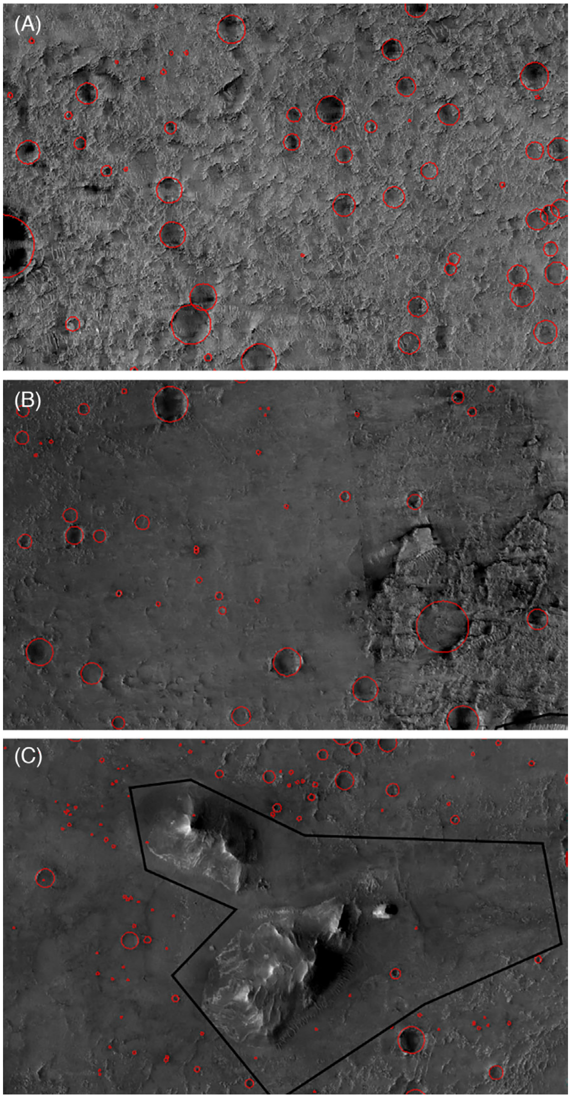

FIGURE 5.13 (A) A subset from the eastern side of the dark-toned (volcanic) floor unit. (B) A subset from the western side of the dark-toned floor unit. (C) An eroded delta deposit. Even though it was identified to be part of the dark-toned floor unit, panel (B) appears more muted and visually resembles the delta deposit in panel (C) more than it resembles the dark-toned unit in (A). This may imply the area in the western part of the dark-toned floor unit was once covered by delta deposits similar to (C) that had nearly completely eroded with time.

burying craters (Sweeney et al., 2018; Day and Dorn, 2019; Warner et al., 2020).

We finally note that in contrast to the visual geomorphological evidence, the crater size distribution shown in Fig. 5.6 may in fact support the hypothesis of contamination by secondaries, due to the apparent excess of craters 100–300 m relative to craters >300 m that follow a younger isochron. It should be noted, however, that the limited number of craters >300 m reduces the statistical significance of this claim.

3.3.3 *How do aeolian erosion and infill affect the crater size distribution?*

Many geologic processes may fade or erase craters: mechanical impact gardening (Gault et al., 1974; Fassett and Thomson, 2014), seismically induced mass wasting (Richardson et al., 2005), exospheric ice (Deutsch et al., 2018; Rubanenko et al., 2019), or volcanic infill (Hartmann, 1999; Edwards et al., 2014). On Mars, erosion is further accelerated by aeolian processes fueled by Mars' atmosphere (Neukum et al., 2001; Hartmann and Neukum, 2001; Smith et al., 2008; Grotzinger and Milliken, 2012; Michael, 2013). In some cases, the crater size distribution preserves erosion and resurfacing events that tend to have a greater effect on the smaller, shallower depressions (as seen, e.g., near Olympus Mons in Fig. 5.3).

On a differential plot the size distribution of an eroded or infilled population of craters appears like a discontinuity, the branches of which follow different production function isochrons, as fresh craters form where previous craters are lost [see, e.g., Figs. 5.6, 5.8, or 5.12, and additional examples in Melosh (1989), Hartmann and Neukum (2001)]. The model age of the older branch may help constrain the age of the unit, while the model age of the younger branch may help constrain the time at which the partial resurfacing event occurred (Michael, 2013).

The effect of resurfacing on the crater age of a geologic unit may be seen by comparing the crater size distributions analyzed earlier: even though the stratigraphic relations interpreted by Goudge et al. (2015) would imply the delta unit precedes the dark-toned floor unit, its eroded or infilled crater size distribution appears to represent a significantly younger retention age. The same is true for the LTF unit, in which aeolian features may have affected the crater size distribution by removing or eroding craters. It is also interesting to note the younger branch of all the surveyed units in Jezero crater follows approximately the same isochron, 10–100 Ma. This may imply a geologic process erased craters on scales <100 m across all the geologic units of Jezero.

Some of the disagreement between this survey and previous surveys (Shahrzad et al., 2019; Schon et al., 2012; Goudge et al., 2012) may stem from the limited count area. Surveying limited count areas increases the statistical uncertainty in the derived model age due to the smaller sample size and the natural spatial variability that exists even within a single geologic unit (Pasckert et al., 2015; Williams et al., 2018). As resurfacing tends to affect smaller craters more than larger craters, its influence grows when the surveyed area is small (Warner et al., 2015). More recent probabilistic models (Palucis et al., 2020) have determined the highest uncertainty occurs for surfaces whose age is ~2 Ga, which is close to the crater age of the dark-toned floor unit. For landscapes that exhibit limited erosion, an accurate surface age may be predicted on the condition that the ratio of the square root of the tested area to the minimum crater diameter does not exceed ~200 (Palucis et al., 2020). This condition is met for our survey of the dark-toned floor unit but not for previous surveys (Shahrzad et al., 2019). However, when considering a moderate erosion rate of 25 nm $year^{-1}$, a much greater minimum area of 10^4 km^2 is required. This should be considered if a sample obtained from the dark-toned floor unit will be used in the future to calibrate Mars's crater chronology.

3.3.4 *How do the target material properties affect crater chronology?*

The previous sections have dealt with the evolution of cratered surfaces over time and the concept of crater retention age. In addition to these challenges, the geological diversity of Mars—a consequence of its prolonged history of surface water and active atmosphere—has led to significant differences in the target material properties of cratered terrains, thereby affecting their formation diameters and size distribution, and the derived retention ages. This is emphasized within fossilized lacustrine systems such as Jezero crater, where sharp boundaries separate morphologically distinct deposits lying side by side on the crater floor.

The target material properties affect the formation process in all three crater formation stages (see Section 2.1). In the compression and excavation stages, denser, bulkier material will naturally better resist the penetrating projectile and the propagating shock wave. In the modification stage, material strength and porosity become important with bedrock retaining the crater transient shape better than loosely packed regolith (Dundas et al., 2010; Stopar et al., 2017).

Physical laws linking the target properties, the impactor energy, and the crater dimensions were first introduced following experiments conducted on controlled TNT explosions (Lampson, 1946; Chabai, 1965). These initial studies led to the current extensive, quasi-experimental crater scaling formalism that links the impact energy and the target properties to the volume of the transient crater V_t formed on the surface, employing Buckingham's π theorem of dimensional analysis (Holsapple and Schmidt, 1987; Schmidt and Housen, 1987; Holsapple, 1993; Richardson, 2009),

$$V_t = K_1\left(\frac{m_i}{\rho_t}\right)\left[\left(\frac{ga_i}{\upsilon_i^2}\right)\left(\frac{\rho_t}{\rho_i}\right)^{-\frac{1}{3}} + \left(\frac{\bar{Y}}{\rho_t\upsilon_i^2}\right)^{\frac{2+\mu}{2}}\right]^{-\frac{3\mu}{2+\mu}} \quad (5.3)$$

where m_i, a_i, υ_i, and ρ_i are the mass, radius, velocity, and density of the impactor; ρ_t is the target material density, g is the acceleration due to gravity; and K_1, $\bar{Y}$, and μ are experimentally derived properties of the target material. $\bar{Y}$ is the target material strength, which has units of pressure, $1/3 < \mu < 2/3$ is a parameter that affects the physical dimensions of the coupling parameter (see Holsapple and Schmidt, 1987) and determines if the impact is governed by the impactor momentum ($\mu = 1/3$) or kinetic energy ($\mu = 2/3$) and K_1 is a proportionality constant. For example, for loose sand $\bar{Y} \sim 0$ Pa, $\mu = 0.41$, and $K_1 = 0.24$ while for hard rock $\bar{Y} \sim 10^7$ Pa, $\mu = 0.55$, and $K_1 = 0.2$. Other typical values for these constants may be found in Holsapple (1993) and Williams et al. (2014). The crater diameter may be obtained by taking the cube root of the volume, $V = \pi D^3/24$.

In order to demonstrate the effect of material strength on the crater size distribution, we use a Monte Carlo model that is based on the Cratered Terrain Evolution Model by Richardson (2009). Our model employs π-scaling (Eq. 5.3) and realistic ejecta (Richardson et al., 2007) to randomly form craters on an initially smooth (without craters) surface and simulate impact-related processes. We choose four example material properties from Holsapple (1993): dry sand, two types of dry soil, and hard rock. For each set of material properties, we form crater populations using the same production function: a power-law impactor size distribution with $b = 2.5$ for 500 Ma (see Section 2.1). In all of the simulations, we set the impactor density to $\rho_i = 1500$ kg m^{-3}, the impact velocity to $\upsilon_i = 20$ km s^{-1} and assume a Martian-like $g = 3.7$ m s^{-2}.

Panel (A) of Fig. 5.14 shows four differential distributions, one for each crater population, along with isochrons from the Ivanov (2001) production function. Even though we employed the same impactor size distribution in forming the craters, their derived age is different by up to two orders of magnitude. In panel (B), we show four snapshots, one from each simulation that demonstrate material properties not only

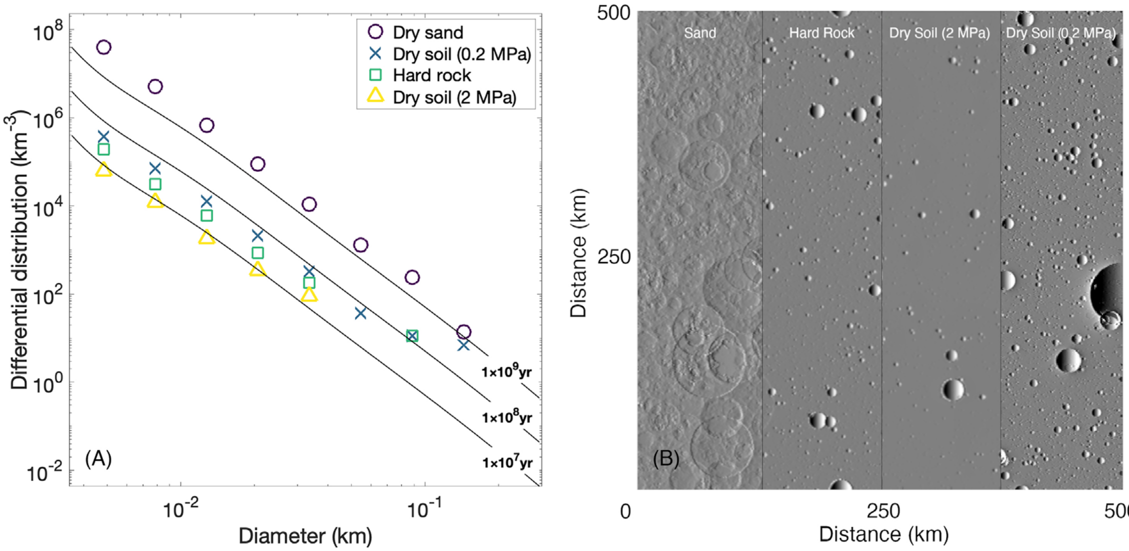

FIGURE 5.14 The effect of material properties on the crater size distribution, and the derived age of the surface. We use our Monte Carlo model to simulate an impactor size distribution with $b = 2.5$ for 500 Ma. The results deviate slightly from the isochrons since the power-law coefficient we employed assumes the impact rate measured for Earth bolides (Brown et al., 2002), corrected for Mars (Le Feuvre and Wieczorek, 2011). We assume an impactor density of $\rho_i = 1500$ kg m^{-3}, an impact velocity of $v_i = 20$ km s^{-1} and $g = 3.7$ m s^{-2}. To simulate targets with different material properties, we use parameters from Holsapple (1993). (A) The crater size distribution for four sets of target properties: dry sand ($\mu = 0.41$, $K_1 = 0.24$, $\bar{Y} = 0$ Pa), two types of dry soil ($\mu = 0.41$, $K_1 = 0.24$, $\bar{Y} = 0.2$ and 2 MPa), and hard rock ($\mu = 0.55$, $K_1 = 0.2$, $\bar{Y} = 20$ MPa), with isochrons drawn from the production function due to Ivanov (2001). Even though the impactor size distribution is identical for all surfaces, the derived age is significantly different. (B) Four snapshots showing part of the simulated 500 Ma old surface. Note the different crater size distribution and morphology in each case. The image panels in (B) only show part of the simulated surface as example and should not be regarded as representative of the complete surface crater size-frequency distribution.

change the crater age but also the morphology of the cratered surface. Our results indicate that the target material properties have a significant effect on the observed crater size distribution—which may help resolve some of the differences between the ages derived from the size distributions we analyzed in Section 3.2.

4 Discussion and conclusions

Mars' history of surface water and active atmosphere invites challenges that interfere with our ability to reliably date its surface through crater counting. Previously we reviewed some of these challenges, adopting as a case study the crater Jezero, the landing site of the Mars 2020 mission. Understanding the size distribution of craters within Jezero is important, as the radiometric age of samples obtained from the basin floor could be used in the future to calibrate crater chronology studies on Mars.

In order to demonstrate how these challenges affect the measured crater size distributions on the floor of Jezero, we have compiled a catalog of 3274 craters complete to ~50–70 m, depending on the surveyed unit (see Fig. 5.11). Our study focused on comparing the age derived from the crater size distributions to the depositional age of the units derived by interpreting the local geology. Employing crater chronology, we have dated three prominent geologic units found within Jezero crater: the dark-toned floor unit, the LTF unit, and the western delta fan unit. Due to the near absence of craters on the northern fan unit, we were not able to reliably derive its crater age.

Of all the geologic units on the floor of Jezero crater, the dark-toned floor best records and preserves impact craters over time. In order to extend the range of craters previously used to date the unit, we employed bootstrapping to better estimate the rollover diameter of the crater size distribution. The crater age we found for the dark-toned floor unit, 2 ± 0.07 Ga, is slightly lower than previous estimates (Shahrzad et al., 2019). This discrepancy, along with recent models showing erosion may significantly alter the crater age of limited count regions (Palucis et al., 2020), should be taken into account when calibrating the crater age of the surface of the dark-toned floor with its measured radiometric age.

In contrast to the geologic evidence, which may indicate the dark-toned floor unit embays the delta fan units, their crater retention age suggests the former is an order of magnitude older than the latter. Previously we have shown that due to extensive erosion, which is in part a function of the material properties, the crater size distribution on the delta fans potentially represents a younger age. This is further bolstered by the presence of Belva crater that matches the ~3 Ga isochron and better agrees with the derived depositional age of the unit. This discrepancy demonstrates well that crater chronology is a proxy of the time duration that a surface has been exposed to impactors, rather than the age of the geologic unit, and should always be incorporated with knowledge about the geology of the target material.

Unlike the delta fan units, which show extensive erosion, craters on the LTF unit are better preserved and should provide a more accurate estimate of the retention age of the unit. However, once again, the derived model age (1.7 ± 0.3 Ga) disagrees with the superposition relationship of the unit determined from images. Here, the differences could be related to the different material strength of the units. Previously we have shown that in some cases the age estimate is heavily influenced by the target material properties that, in the case of craters ~10–100 m, could differ by up to an order of magnitude. This again demonstrates the large errors that may be associated with dating cratered terrains without estimates of the target material properties.

Previously, it was postulated (Shahrzad et al., 2019) that the large variability in crater density on the floor of Jezero may be related to the presence of a cluster of secondaries. In order to test this hypothesis, we inspected the morphology of craters on the floor of Jezero but found no clusters or crater chains. Additionally, craters in the area do not appear more elliptical, or located near a large recent primary crater. Instead, we suggest the difference in crater density on the floor of Jezero is probably related to the geology of the delta units. The tone and morphology of the areas with the lowest crater density in Jezero resemble the surface surrounding the delta fan units. This puzzling line of evidence may suggest the west delta fan extended well inside Jezero, protecting the floor underneath it or that the superpositional relationships between the dark-toned floor unit and the delta units are not yet entirely known. It is also likely that wind currents within the basin lofted material that partially covered or buried small craters found east of the delta fragments (see Fig. 5.5).

Curiously, the differential distribution of all cratered units within Jezero shares a younger power-law branch in their size-frequency distribution between ~10 and 100 m. This observation is puzzling and may indicate a widespread geologic resurfacing process has recently (~100 Ma) occurred in the crater on a large scale. We note that such an event would have to be significant in order to erase these ~50 m craters—the initial depth of which was likely ~5–10 m but are unable to present evidence to help us constrain its nature.

Acknowledgments

The authors wish to thank Nicholas Warner and an anonymous reviewer for helpful feedback and discussion. The contributions of J.-P. Williams were funded by a NASA Solar System Workings grant no. 80NSSC18K0010.

References

Anders, E., 1965. Fragmentation history of asteroids. Icarus 4 (4), 399–408.

Baldwin, R.B., 1981. On the origin of the planetesimals that produced the miltiringed basins. In: Schultz, P., Merrill, R.B. (Eds.), Multi-Ring Basins, Proc. Lun. Planet. Sci. 12A, Pergamon Press, New York, pp. 19–28.

Baldwin, R.B., 1949. The Face of the Moon, University of Chicago Press, Chicago, vol. 42, 114–153, 191.

Barata, T., Alves, E.I., Saraiva, J., Pina, P., 2004. Automatic recognition of impact craters on the surface of Mars. In: Campilho, A., Kamel, M. (Eds.), Image Analysis and Recognition. ICIAR 2004. Lecture Notes in Computer Science, vol. 3212. Springer, Berlin, Heidelberg. https://doi.org/10.1007/978-3-540-30126-4_60.

Baum, M., Wordsworth, R., 2020. Jezero crater and timing of an early Martian ocean. LPI (2326), 2490.

Bierhaus, E., McEwen, A.S., Robbins, S., Singer, K., Dones, L., Kirchoff, M., Williams, J.-P., 2018. Secondary craters and ejecta across the solar system: populations and effects on impact-crater–based chronologies. Meteorit. Planet. Sci. 53 (4), 638–671.

Bierhaus, E.B., Chapman, C.R., Merline, W.J., 2005. Secondary craters on Europa and implications for cratered surfaces. Nature 437 (7062), 1125–1127.

Blasius, K.R., 1976. The record of impact cratering on the great volcanic shields of the Tharsis region of Mars. Icarus 29 (3), 343–361.

Brown, H., 1960. The density and mass distribution of meteoritic bodies in the neighborhood of the earth's orbit. J. Geophys. Res. 65 (6), 1679–1683.

Brown, P., Spalding, R., ReVelle, D.O., Tagliaferri, E., Worden, S., 2002. The flux of small near-earth objects colliding with the earth. Nature 420 (6913), 294.

Cabrol, N.A., Grin, E.A., 1999. Distribution, classification, and ages of Martian impact crater lakes. Icarus 142 (1), 160–172.

Chabai, A.J., 1965. On scaling dimensions of craters produced by buried explosives. J. Geophys. Res. 70 (20), 5075–5098.

Chappelow, J.E., Sharpton, V.L., 2006. Atmospheric variations and meteorite production on Mars. Icarus 184 (2), 424–435.

Crater Analysis Techniques Working Group, 1979. Standard techniques for presentation and analysis of crater size-frequency data. Icarus 37 (2), 467–474.

Day, M., Dorn, T., 2019. Wind in Jezero crater, Mars. Geophys. Res. Lett. 46 (6), 3099–3107.

De Hon, R., 1992. Martian lake basins and lacustrine plains. Earth Moon Planets 56 (2), 95–122.

Deutsch, A.N., Head, J.W., Chabot, N.L., Neumann, G.A., 2018. Constraining the thickness of polar ice deposits on mercury using the mercury laser altimeter and small craters in permanently shadowed regions. Icarus 305, 139–148.

Dobrea, E.N., Stoker, C., Berman, D., McKay, C., Davila, A., 2020. Crater morphology and evolution at the phoenix landing site: insights into timing of modern geological processes and subsurface ice. Icarus 342, 113534.

Dundas, C.M., Keszthelyi, L.P., Bray, V.J., McEwen, A.S., 2010. Role of material properties in the cratering record of young platy-ridged lava on Mars. Geophys. Res. Lett. 37, p. 12203, 10.1029/2010GL042869.

Edgett, K.S., Malin, M.C. 2014. Heavily-cratered sedimentary rock occurrences at the surface of mars, In: GSA Annual Meeting in Vancouver, British Columbia Program, vol. 46, 202–1.

Edwards, C., Bandfield, J., Christensen, P., Rogers, A., 2014. The formation of infilled craters on Mars: evidence for widespread impact induced decompression of the early Martian mantle? Icarus 228, 149–166.

Efron, B., Tibshirani, R., 1985. The bootstrap method for assessing statistical accuracy. Behaviormetrika 12 (17), 1–35.

Ehlmann, B.L., Mustard, J.F., Fassett, C.I., Schon, S.C., Head, III, J.W., Des Marais, D.J., Grant, J.A., Murchie, S.L., 2008. Clay minerals in delta deposits and organic preservation potential on Mars. Nat. Geosci. 1 (6), 355.

Fassett, C.I., Head, III, J.W., 2005. Fluvial sedimentary deposits on Mars: ancient deltas in a crater lake in the Nili Fossae region. Geophys. Res. Lett. 32, p. L14201.

Fassett, C.I., Thomson, B.J., 2014. Crater degradation on the lunar maria: topographic diffusion and the rate of erosion on the moon. J. Geophys. Res. Planets 119 (10), 2255–2271.

Fujiwara, A., Tsukamoto, A., 1980. Experimental study on the velocity of fragments in collisional breakup. Icarus 44 (1), 142–153.

Gault, D., Höorz, F., Brownlee, D., and Hartung, J. 1974. Mixing of the lunar regolith. In Lunar and Planetary Science Conference Proceedings, vol. 5, pp. 2365–2386.

Golder, K., Miklusicak, N., Spaulding, R., Atkins, J., Boring, B., Hicks, T., Shaver, E., Kah, L., 2020. Behavioral characteristics of dark-toned crater floor materials, Jezero crater: implications for mode of emplacement. LPI (2326), 1302.

Goudge, T.A., Head, J.W., Mustard, J.F., Fassett, C.I., 2012. An analysis of openbasin lake deposits on Mars: evidence for the nature of associated lacustrine deposits and post-lacustrine modification processes. Icarus 219 (1), 211–229.

Goudge, T.A., Milliken, R.E., Head, J.W., Mustard, J.F., Fassett, C.I., 2017. Sedimentological evidence for a deltaic origin of the western fan deposit in Jezero crater, Mars and implications for future exploration. Earth Planet. Sci. Lett. 458, 357–365.

Goudge, T.A., Mohrig, D., Cardenas, B.T., Hughes, C.M., Fassett, C.I., 2018. Stratigraphy and paleohydrology of delta channel deposits, Jezero crater, Mars. Icarus 301, 58–75.

Goudge, T.A., Mustard, J.F., Head, J.W., Fassett, C.I., Wiseman, S.M., 2015. Assessing the mineralogy of the watershed and fan deposits of the Jezero crater paleolake system, Mars. J. Geophys. Res. Planets 120 (4), 775–808.
Grant, J.A., Golombek, M.P., Wilson, S.A., Farley, K.A., Williford, K.H., Chen, A., 2018. The science process for selecting the landing site for the 2020 Mars rover. Planet. Space Sci. 164, 106–126.
Greeley, R., Gault, D.E., 1970. Precision size-frequency distributions of craters for 12 selected areas of the lunar surface. Moon 2 (1), 10–77.
Greeley, R., Gault, D.E., 1971. Endogenetic craters interpreted from crater counts on the inner wall of Copernicus. Science 171 (3970), 477–479.
Grotzinger, J.P., Milliken, R.E., 2012. The sedimentary rock record of Mars: distribution, origins, and global stratigraphy. Sediment. Geol. Mars 102, 1–48.
Hartmann, W., 1964. On the distribution of lunar crater diameters. Commun. Lunar Planet. Lab. 2, 197–204.
Hartmann, W., Daubar, I., 2017. Martian cratering 11. utilizing decameter scale crater populations to study Martian history. Meteorit. Planet. Sci. 52 (3), 493–510.
Hartmann, W.K., 1966. Martian cratering. Icarus 5 (1–6), 565–576.
Hartmann, W.K., et al., 1981. Chronology of Planetary Volcanism by Comparative Studies of Planetary Craters, Basaltic Volcanism on the Terrestrial Planets, Pergamon Press, Elmsford, NY, pp. 1050–1127.
Hartmann, W.K., 1999. Martian cratering VI: crater count isochrons and evidence for recent volcanism from Mars global surveyor. Meteorit. Planet. Sci. 34 (2), 167–177.
Hartmann, W.K., 2005. Martian cratering 8: isochron refinement and the chronology of Mars. Icarus 174 (2), 294–320.
Hartmann, W.K., Hartmann, A.C., 1968. Asteroid collisions and evolution of asteroidal mass distribution and meteoritic flux. Icarus 8 (1–3), 361–381.
Hartmann, W.K., Neukum, G., 2001. Cratering chronology and the evolution of Mars. In: Kallenbach R., Geiss J., Hartmann W.K. (Eds.) Chronology and Evolution of Mars. Space Sciences Series of ISSI, vol. 12. Springer, Dordrecht. https://doi.org/10.1007/978-94-017-1035-0_6.
Hawkins, G.S., 1960. Asteroidal fragments. Astron. J. 65, 318.
Holsapple, K., 1993. The scaling of impact processes in planetary sciences. Annu. Rev. Earth Planet. Sci. 21 (1), 333–373.
Holsapple, K., Schmidt, R., 1987. Point source solutions and coupling parameters in cratering mechanics. J. Geophys. Res. Solid Earth 92 (B7), 6350–6376.
Irwin, R.P., Zimbelman, J.R., 2012. Morphometry of Great Basin pluvial shore landforms: Implications for paleolake basins on Mars. J. Geophys. Res. 117, E07004.
Ivanov, B., Deniem, D., Neukum, G., 1997. Implementation of dynamic strength models into 2d hydrocodes: Applications for atmospheric breakup and impact cratering. Int. J. Impact Eng. 20 (1–5), 411–430.
Ivanov, B.A., 2001. Mars/moon cratering rate ratio estimates. Space Sci. Rev. 96 (1–4), 87–104.
Kah, L., Scheller, E., Eide, S., Meyen, F., Jacob, S., Spaulding, R., Miklusicak, N., Golder, K., Stack-Morgan, K., 2020. Depositional relationships between crater floor materials in Jezero crater, Mars. LPI, (2326), 1301.
Kreiter, T., 1960. Dating lunar surface features by using crater frequencies. Publ. Astron. Soc. Pac. 72 (428), 393–398.
Lampson, C.J., 1946. Explosions in earth. In Effects of Impact and explosion V.1, Chap. 3, p. 110. Washington, DC: Off. Sci. Res. Dev.
Lapôtre, M.G., Ielpi, A., 2020. The pace of fluvial meanders on Mars and implications for the western delta deposits of Jezero crater. AGU Adv. 1 (2), e2019AV000141.
Le Feuvre, M., Wieczorek, M.A., 2011. Nonuniform cratering of the moon and a revised crater chronology of the inner solar system. Icarus 214 (1), 1–20.
Lorenz, R.D., Lunine, J.I., 1996. Erosion on titan: past and present. Icarus 122 (1), 79–91.
Mainzer, A., Grav, T., Masiero, J., Bauer, J., Cutri, R., McMillan, R., Nugent, C., Tholen, D., Walker, R., Wright, E., 2012. Physical parameters of asteroids estimated from the wise 3-band data and NEOWISE post-cryogenic survey. Astrophys. J. Lett. 760 (1), L12.
Malin, M.C., Bell, J.F., Cantor, B.A., Caplinger, M.A., Calvin, W.M., Clancy, R.T., Edgett, K.S., Edwards, L., Haberle, R.M., James, P.B., et al., 2007. Context camera investigation on board the Mars Reconnaissance Orbiter. J. Geophys. Res. Planets 112 (E5), E05S04.
Malin, M.C., Edgett, K.S., Cantor, B.A., Caplinger, M.A., Danielson, G.E., Jensen, E.H., Ravine, M.A., Sandoval, J.L., Supulver, K.D., 2010. An overview of the 1985-2006 Mars orbiter camera science investigation. Mars 5, 1–60.
Marchi, S., Mottola, S., Cremonese, G., Massironi, M., Martellato, E., 2009. A new chronology for the moon and mercury. Astron. J. 137 (6), 4936.
Massey, F.J., 1951. The Kolmogorov-Smirnov test for goodness of fit. J. Am. Stat. Assoc. 46 (253), 68–78.
McEwen, A.S., Eliason, E.M., Bergstrom, J.W., Bridges, N.T., Hansen, C.J., Delamere, W.A., Grant, J.A., Gulick, V.C., Herkenhoff, K.E., Keszthelyi, L., et al., 2007. Mars Reconnaissance Orbiter's High Resolution Imaging Science Experiment (HiRISE). J. Geophys. Res. Planets 112 (E5).
McEwen, A.S., Banks, M.E., Baugh, N., Becker, K., Boyd, A., Bergstrom, J.W., Beyer, R.A., Bortolini, E., Bridges, N.T., Byrne S., Castalia, B., Chuang, F.C., Crumpler, L.S., Daubar I., Davatzes, A.K., Deardorff, D.G., DeJong A., Delamere, W.A., Dobrea, E.N., Dundas, C.M., Eliason, E.M., Espinoza, Y., Fennema, A., Fishbaugh, K.E. Forrester, T., Geissler, P.E., Grant, J.A., Griffes, J.L., Grotzinger, J.P., Gulick, V.C., Hansen, C.J., Herkenhoff, K.E., Heyd, R., Jaeger, W.L., Jones D., Kanefsky, B., Keszthelyi, L., King, R., Kirk, R.L., Kolb, K.J., Lasco, J., Lefort A., Leis, R., Lewis, K.W., Martinez-Alonso, S., Mattson, S., McArthur G., Mellon, M.T., Metz, J.M., Milazzo, M.P., Milliken,

R.E., Motazedian, T., Okubo, C.H., Ortiz, A., Philippoff, A.J., Polit, J.A., Russell, P.S., Schaller, C., Searls, M.L., Spriggs, T., Squyres, S.W., Tarr, S., Thomas, N., Thomson, B.J., Tornabene, L.L., Houten, C.V., Verba, C., Weitz, C.M., Wray, J.J., 2010. The High Resolution Imaging Science Experiment (HiRISE) during MRO's Primary Science Phase (PSP), Icarus, 205(1), pp. 2–37.

Melosh, H.J., 1989. Impact Cratering: A Geologic Process. Oxford University Press, New York, N.Y.

Michael, G., 2013. Planetary surface dating from crater size–frequency distribution measurements: multiple resurfacing episodes and differential isochron fitting. Icarus 226 (1), 885–890.

Michael, G., Kneissl, T., Neesemann, A., 2016. Planetary surface dating from crater size-frequency distribution measurements: poisson timing analysis. Icarus 277, 279–285.

Michael, G., Neukum, G., 2010. Planetary surface dating from crater size–frequency distribution measurements: partial resurfacing events and statistical age uncertainty. Earth Planet. Sci. Lett. 294 (3–4), 223–229.

Milton, D.J., 1973. Water and processes of degradation in the Martian landscape. J. Geophys. Res. 78 (20), 4037–4047.

Neukum, G., 1984. Meteorite bombardment and dating of planetary surfaces. National Aeronautics and Space Administration, Thesis—February 1983, Washington, DC. Translated into English of "Meteoritenbombardement und Datierung Planetarer Oberflaechen" Munich, February 1983, pp. 1–186.

Neukum, G., Ivanov, B.A., 1994. In: Gehrels, T. (Ed.), Hazards Due to Comets and Asteroids, University of Arizona Press, Tucson, AZ, pp. 359–416.

Neukum, G., Ivanov, B.A., Hartmann, W.K., 2001. Cratering Records in the Inner Solar System in Relation to the Lunar Reference System. In: Kallenbach, R., Geiss, J., Hartmann, W.K. (Eds.), Chronology and Evolution of Mars. Space Sciences Series of ISSI, vol 12. Springer, Dordrecht. https://doi.org/10.1007/978-94-017-1035-0_3.

Neukum, G., Ǩonig, B., Fechtig, H., and Storzer, D. (1975). Cratering in the earth-moon system-consequences for age determination by crater counting. In Lunar and Planetary Science Conference Proceedings, vol. 6, pp. 2597–2620.

Palucis, M.C., Jasper, J., Garczynski, B., Dietrich, W.E., 2020. Quantitative assessment of uncertainties in modeled crater retention ages on Mars. Icarus 341, 113623.

Pasckert, J.H., Hiesinger, H., van der Bogert, C.H., 2015. Small-scale lunar farside volcanism. Icarus 257, 336–354.

Popova, O., Nemtchinov, I., Hartmann, W.K., 2003. Bolides in the present and past Martian atmosphere and effects on cratering processes. Meteorit. Planet. Sci. 38 (6), 905–925.

Preblich, B.S., McEwen, A.S., Studer, D.M., 2007. Mapping rays and secondary craters from the Martian crater Zunil. J. Geophys. Res. Planets 112, E05006.

Quantin, C., Popova, O., Hartmann, W.K., Werner, S.C., 2016. Young Martian crater Gratteri and its secondary craters. J. Geophys. Res. Planets 121 (7), 1118–1140.

Rabinowitz, D., 1993. The size distribution of the earth-approaching asteroids. Astrophys. J. 407, 412–427.

Richardson, J.E., 2009. Cratering saturation and equilibrium: a new model looks at an old problem. Icarus 204 (2), 697–715.

Richardson, J.E., Melosh, H.J., Lisse, C.M., Carcich, B., 2007. A ballistics analysis of the deep impact ejecta plume: Determining comet Tempel 1's gravity, mass, and density. Icarus 191 (2), 176–209.

Richardson, Jr., J.E., Melosh, H.J., Greenberg, R.J., O'Brien, D.P., 2005. The global effects of impact-induced seismic activity on fractured asteroid surface morphology. Icarus 179 (2), 325–349.

Robbins, S.J., 2019. A new global database of lunar impact craters >1-2 km: 1. Crater locations and sizes, comparisons with published databases, and global analysis. J. Geophys. Res. Planets 124 (4), 871–892.

Robbins, S.J., Hynek, B.M., 2011. Secondary crater fields from 24 large primary craters on Mars: insights into nearby secondary crater production. J. Geophys. Res. Planets 116 (E10).

Robbins, S.J., Hynek, B.M., 2012. A new global database of Mars impact craters ≥1 km: 1. Database creation, properties, and parameters. J. Geophys. Res. 117, E05004, doi:10.1029/2011JE003966.

Robbins, S.J., Hynek, B.M., 2012. A new global database of Mars impact craters ≥1 km: 2. Global crater properties and regional variations of the simple-to-complex transition diameter. J. Geophys. Res. 117, E06001, doi:10.1029/2011JE003967.

Robbins, S.J., Hynek, B.M., 2014. The secondary crater population of Mars. Earth Planet. Sci. Lett. 400, 66–76.

Rubanenko, L., Venkatraman, J., Paige, D.A., 2019. Thick ice deposits in shallow simple craters on the moon and mercury. Nat. Geosci. 12 (8), 597–601.

Salese, F., Kleinhans, M.G., Mangold, N., Ansan, V., McMahon, W., de Haas, T., Dromart, G., 2020. Astrobiology 20. 977–993.

Schmidt, R.M., Housen, K.R., 1987. Some recent advances in the scaling of impact and explosion cratering. Int. J. Impact Eng. 5 (1–4), 543–560.

Schon, S.C., Head, J.W., Fassett, C.I., 2012. An overfilled lacustrine system and progradational delta in Jezero crater, Mars: implications for Noachian climate. Planet. Space Sci. 67 (1), 28–45.

Schultz, P. H. and Singer, J. (1980). A comparison of secondary craters on the moon, mercury, and mars. In Lunar and Planetary Science Conference Proceedings, vol. 11, pp. 2243–2259.

Schuyler, A., Warner, N., Derick, B., Rogers, A., Golombek, M., 2020. Crater morphometry on the dark-toned mafic floor unit at Jezero crater, Mars: Comparisons to a known basaltic lava plain at the insight landing site. LPI (2326), 1608.

Shahrzad, S., Kinch, K.M., Goudge, T.A., Fassett, C.I., Needham, D.H., Quantin-Nataf, C., Knudsen, C.P., 2019. Crater statistics on the dark-toned, mafic floor unit in Jezero crater, Mars. Geophys. Res. Lett. 46 (5), 2408–2416.

Shoemaker, E.M., 1965. Preliminary analysis of the fine structure of the lunar surface in Mare Cognitum, in Ranger VII. Part 2. Experimenters' Analyses and Interpretations. Jet Propulsion Laboratory, California Institute of Technology, Technical Report No. 32–700, pp. 75–134.

Silburt, A., Ali-Dib, M., Zhu, C., Jackson, A., Valencia, D., Kissin, Y., Tamayo, D., Menou, K., 2019. Lunar crater identification via deep learning. Icarus 317, 27–38.

Smith, D.E., Zuber, M.T., Frey, H.V., Garvin, J.B., Head, J.W., Muhleman, D.O., Pettengill, G.H., Phillips, R.J., Solomon, S.C., Zwally, H.J., et al., 2001. Mars orbiter laser altimeter: experiment summary after the first year of global mapping of Mars. J. Geophys. Res. Planets 106 (E10), 23689–23722.

Smith, M.R., Gillespie, A.R., Montgomery, D.R., 2008. Effect of obliteration on crater-count chronologies for Martian surfaces. Geophys. Res. Lett. 35 (10), L10202, doi:10.1029/2008GL033538.

Soderblom, L., Condit, C., West, R.A., Herman, B., Kreidler, T., 1974. Martian planetwide crater distributions: implications for geologic history and surface processes. Icarus 22 (3), 239–263.

Spencer, L.J., 1937. Meteorites and the craters on the moon. Nature 139, 655–657.

Stepinski, T.F., Mendenhall, M.P., Bue, B.D., 2009. Machine cataloging of impact craters on Mars. Icarus 203 (1), 77–87.

Stöffler, D., Ryder, G., 2001. Stratigraphy and Isotope Ages of Lunar Geologic Units: Chronological Standard for the Inner Solar System. In: Kallenbach, R., Geiss, J., Hartmann, W.K. (eds) Chronology and Evolution of Mars. Space Sciences Series of ISSI, vol. 12. Springer, Dordrecht. https://doi.org/10.1007/978-94-017-1035-0_2.

Stopar, J.D., Robinson, M.S., Barnouin, O.S., McEwen, A.S., Speyerer, E.J., Henriksen, M.R., Sutton, S.S., 2017. Relative depths of simple craters and the nature of the lunar regolith. Icarus 298, 34–48.

Strom, R.G., Banks, M.E., Chapman, C.R., Fassett, C.I., Forde, J.A., Head, III, J.W., Merline, W.J., Prockter, L.M., Solomon, S.C., 2011. Mercury crater statistics from messenger flybys: implications for stratigraphy and resurfacing history. Planet. Space Sci. 59 (15), 1960–1967.

Stuart, J.S., Binzel, R.P., 2004. Bias-corrected population, size distribution, and impact hazard for the near-earth objects. Icarus 170 (2), 295–311.

Sweeney, J., Warner, N., Ganti, V., Golombek, M., Lamb, M., Fergason, R., Kirk, R., 2018. Degradation of 100-m-scale rocky ejecta craters at the insight landing site on Mars and implications for surface processes and erosion rates in the Hesperian and Amazonian. J. Geophys. Res. Planets 123 (10), 2732–2759.

Warner, N., Grant, J., Wilson, S., Golombek, M., DeMott, A., Charalambous, C., Hauber, E., Ansan, V., Weitz, C., Pike, T., et al., 2020. An impact crater origin for the insight landing site at homestead hollow, Mars: implications for near surface stratigraphy, surface processes, and erosion rates. J. Geophys. Res. Planets 125 (4), e2019JE006333.

Warner, N.H., Gupta, S., Calef, F., Grindrod, P., Boll, N., Goddard, K., 2015. Minimum effective area for high resolution crater counting of Martian terrains. Icarus 245, 198–240.

Wilhelms, D. (1976). Secondary impact craters of lunar basins. In Lunar and Planetary Science Conference Proceedings, vol. 7, pp. 2883–2901.

Williams, J.-P., Pathare, A.V., Aharonson, O., 2014. The production of small primary craters on Mars and the moon. Icarus 235, 23–36.

Williams, J.-P., van der Bogert, C.H., Pathare, A.V., Michael, G.G., Kirchoff, M.R., Hiesinger, H., 2018. Dating very young planetary surfaces from crater statistics: a review of issues and challenges. Meteorit. Planet. Sci. 53 (4), 554–582.

Williford, K.H., Farley, K.A., Stack, K.M., Allwood, A.C., Beaty, D., Beegle, L.W., Bhartia, R., Brown, A.J., de la Torre Juarez, M., Hamran, S.-E., et al., 2018. The NASA Mars 2020 rover mission and the search for extraterrestrial life. From Habitability to Life on Mars. Elsevier, Amsterdam, Netherlands, pp. 275–308.

Young, J., 1940. A statistical investigation of diameter and distribution of lunar craters. J. Br. Astron. Assoc. 50 (9), 309–326.